Unveiling the influence of interfacial bonding and dynamics on solid/liquid interfacial structures: An *ab initio* molecular dynamics study of (0001) sapphire-liquid Al interfaces

Sida Ma[1,2] Rui Yan,[1] Nanfu Zong,[1] Ruslan L. Davidchack[2,*] Tao Jing,[1,†] and Hongbiao Dong[3]

[1]*School of Materials Science and Engineering, Tsinghua University, Beijing 100084, China*

[2]*Department of Mathematics, University of Leicester, Leicester, LE1 7RH, United Kingdom*

[3]*Department of Engineering, University of Leicester, Leicester, LE1 7RH, United Kingdom*

(Received 27 November 2019; accepted 13 January 2020; published 4 February 2020)

Nucleant substrates may induce formation of several quasilayers in the liquid metals in contact with the solid substrates. These liquid layers, called prenucleation layers (PNLs), normally form above the liquidus temperatures of the metal alloys and thus are believed to significantly affect the heterogeneous nucleation mechanism. In this work, a comprehensive study of the (0001) sapphire-liquid Al interfaces was conducted using the *ab initio* molecular dynamics method to unveil the key factors determining the substrate-liquid metal interfacial structural features, focusing primarily on revealing the underlying mechanisms of the PNL formation. Two types of (0001) sapphire surfaces, i.e., nonhydroxylated and hydroxylated surfaces, were investigated. Essentially the same equilibrated interfacial structure was observed for all the interfaces with the nonhydroxylated sapphire surfaces, featuring an Al-rich termination of the substrates and two distinguishable adjacent PNLs. These typical structural features are similar to the $(\sqrt{31} \times \sqrt{31})R \pm 9^\circ$ reconstructed surface, which supports the previous experimental observation that the presence of liquid Al promotes the reconstruction of the (0001) sapphire surface. A completely different structure was found at the interface with fully hydroxylated sapphire surface: the PNLs are absent, replaced by an Al-depleted region. To unveil the factors influencing the interfacial structure, we first analyzed the nature of interfacial bonding. Strong covalent bonds were observed between the nonhydroxylated sapphire surfaces and liquid Al, which constitute a relatively large proportion of the interfacial bonds at such systems. On the contrary, weak van der Waals force is the primary interaction between the fully hydroxylated sapphire surface and liquid Al. Then we characterized the dynamical behaviors of the substrate surfaces in the substrate-liquid Al interfaces. Better mobility and larger vibration amplitude were found for the fully hydroxylated sapphire surface compared to the equilibrated nonhydroxylated sapphire surface. We demonstrated that both the stronger bonding strength and the lower mobility of interfacial atoms contribute to the formation of the PNLs at the nonhydroxylated sapphire-liquid Al interfaces. Finally, the formation mechanism of the PNLs at the substrate-liquid metal interface is summarized.

DOI: 10.1103/PhysRevMaterials.4.023401

I. INTRODUCTION

Layering of liquid metals in the proximity of a substrate surface has drawn great attention in recent years due to its importance from both practical [1–5] and theoretical [6–14] points of view. A wide variety of technological applications, such as grain refinement by nucleating agents [1–3], thermal energy storage by the metal/oxide core-shell nanoparticles [4], epitaxial growth or heterogeneous catalysis by the ceramic substrates [5,15], lubrication [16], etc., are all influenced by the liquid layering. Additionally, further investigation of this physical phenomenon is critical to a thorough understanding of the heterogeneous nucleation mechanisms [17–23], which are of fundamental importance in the theoretical study of liquid-solid phase transformations.

In the widely used classical nucleation theory (CNT) [17], the possible medium- or long-range order [24] of melts, particularly when they are in contact with a substrate, is ignored. Therefore, the phenomenon of liquid layering near a nucleant [4–6,8,25–34] above the liquidus temperature (T_m) is difficult to account for within the CNT framework. At the same time, recent experimental and modeling research indicates that the prenucleation layers (PNLs), the quasicrystal layers formed in the liquid near a nucleant substrate above T_m, play a key role in determining the heterogeneous nucleation behavior and efficiency [28,35,36]. So, it is imperative to investigate the details of the structural features of the interfaces present during heterogeneous nucleation in order to develop a comprehensive understanding of the connection between the PNLs and the heterogeneous nucleation mechanisms. In addition, elucidating the mechanism of the PNLs formation and determining the factors controlling the characteristics of the PNLs are important for better understanding the properties of the substrate-liquid metal interfacial structures.

External environment, such as temperature and pressure, and internal factors, such as structural [12,13,37,38] and chemical [39–43] features of the nucleant substrate, etc., significantly affect the structure of the interfaces present at nucleation. After the appearance of the PNLs, the interface between a liquid metal and a substrate may be strained,

*rld8@leicester.ac.uk

†jingtao@mail.tsinghua.edu.cn

 ©2020 American Physical Society

which is determined by the structural difference between the substrate and the PNLs. The structural difference is normally quantified by explicitly calculating the interfacial lattice mismatch f. The two-dimensional (2D) lattice misfit model proposed by Bramfitt [44] and the edge-to-edge matching model of Zhang and Kelly [45] are well-accepted models to calculate f. Interfacial lattice mismatch has been employed as a criterion to search for grain refiners for metal casting in industry [12,37,38,45–48]. Smaller f means closer structural features between the refiner and the crystalline metal, which is believed to be beneficial to heterogeneous nucleation. A number of successful examples show the efficiency of the f criterion in predicting possible grain refiners for Al alloys [48], Mg alloys [45–47], Fe alloys [38], etc. The f criterion can be also applied in predicting the structural features of the PNLs: the smaller f (between the substrate and the PNLs) is, the higher propensity for the PNLs to form. However, such an analysis is much too simplified, since it neglects the chemical composition and dynamical properties of the solid/liquid interfaces. Taking a closer look at the formation process of the PNLs, we should note that the interfacial strain energy, quantified by the value of f, is the barrier for the PNL formation. Besides, the ordering of liquid atoms in the PNLs at a temperature above T_m is also not energetically favorable, since it increases the volumetric Gibbs free energy of the system. Hence, a driving force is still required for the PNLs to appear. The driving force may originate from the substrate-liquid metal interaction, which could create more chemical bonds at the interface, thus reducing the interfacial chemical free energy. Therefore, it is also necessary to place more emphasis on the influence of bonding features on the interfacial structures, especially the formation of the PNLs.

It is also worth noting that change of atomic configuration of the substrate surface or addition of alloying elements in the liquid metal could substantially affect the bonding features at the substrate-liquid metal interface and thus should be combined with the lattice mismatch models [12,38,44–46] to predict the structures of the interface. In addition, new insight into the alloying effects (such as Zr poisoning [49] with respect to the Al-Ti-B refiners or the tuning of heterogeneous nucleation of Al on the sapphire substrate by the addition of Cu solutes [13,50]) is expected to be gained from further investigation of the role of bonding in influencing the structural features of the substrate-liquid metal interfaces. The above discussion emphasizes the fundamental importance of bonding analysis in predicting the interfacial characteristics that are vital effective selection or design of grain refiners for a specified metal alloy.

Apart from the bonding features, the dynamical properties, such as the vibration or diffusion of the substrate surface atoms or the diffusion of the liquid metal atoms near the surface, would also greatly change the structural properties of the interface. As demonstrated in our previous studies [35,36], the PNLs have structures that are greatly influenced by the substrate, yet their dynamical properties show more similarity to the liquid metal. This implies that the stiffness and viscosity of the PNLs are much weaker compared to those of the solid substrate. Therefore, substrate surface atom vibrations with large amplitude (or their diffusion, which leads to atomic-scale surface roughness) will definitely alter the interfacial structures, and the PNLs may even be destroyed under such conditions. Hence, it is also necessary to pay more attention to the role of interfacial vibrations in altering the substrate-liquid metal interfaces.

To serve as a good nucleant for liquid metals, the substrate should at least remain undissolved when it is brought into contact with the liquid metal. Accordingly, oxides [51], borides [2], carbides [52], and some intermetallic compounds [1] with high melting temperatures are considered to be potential nucleant substrates for metal alloys. In this work, the sapphire (α-Al_2O_3) substrate is chosen as a typical example to study its interfaces with liquid Al. Sapphire is selected due to the following three reasons: (1) its interfaces with liquid Al represent the typical bonding features in most of the substrate-liquid metal interfaces where the transition from the covalent/ionic bonds in the bulk substrates to the metallic bonds in the bulk liquid metal is expected; (2) the (0001) sapphire surface has a variety of terminations with different atomic configurations (Fig. 1) [53–56], which may bond differently with liquid Al, thus exhibiting distinct interfacial structures; (3) the (0001) sapphire-liquid Al interface has been extensively explored using a variety of experimental techniques [5,11,13,26,35,57], and the existence of the PNLs was confirmed in these experimental studies [5,35], which provides a solid basis for further studies of the mechanisms of PNL formation.

Using the high-resolution transmission electron microscopy (HRTEM) and the surface x-ray diffraction (SXRD)

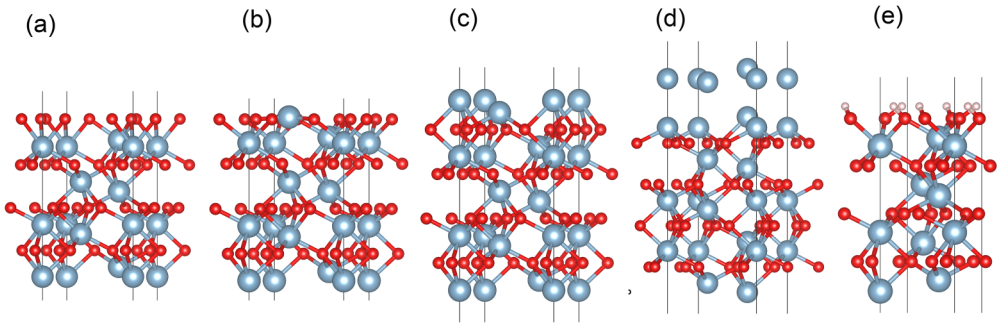

FIG. 1. Five different (0001) sapphire surface terminations used in the AIMD simulations. (a) O terminated; (b) 1Al terminated; (c) 2Al terminated; (d) reconstructed; (e) fully hydroxylated. The large gray spheres are Al atoms, the small red spheres are O atoms, and the smallest white spheres are H atoms.

[58,59] respectively, Oh *et al.* [5] and Ma *et al.* [35] detected stratified liquid Al structures in the vicinity of the (0001) sapphire substrate. The degree of order of these quasiliquid layers (which were observed at temperatures above T_m and thus were confirmed to be the aforementioned PNLs) decays rapidly with increasing distance to the substrate. Although the HRTEM and SXRD approaches may provide opportunities to detect the substrate-liquid metal interfaces at the atomic scale, they both have obvious drawbacks which limit their applications. For the SXRD, only the crystalline substrates show distinguishable crystal truncation rod (CTR) [60], which is then mapped to the interfacial atomic arrangement by fitting the CTR data to specific interface models [61]. Also, hydrogen atoms are difficult to detect by this technique [62], which limits its use for characterization of the hydroxylated interfaces. For HRTEM, the electron irradiation damage of the ceramics at an elevated temperature cannot be ignored [5]. Additionally, it is difficult to distinguish the atomic species in such experiments. According to our previous studies, the PNLs at the (0001) sapphire-liquid Al interface form within about 20 picoseconds (ps), which is far shorter than the timescales of the aforementioned experimental methods. Furthermore, both the SXRD and HRTEM experiments are much better at structural characterization than at analyzing the bonding or dynamical features at an interface. Hence, it would be extremely difficult to use experimental approaches to analyze the influence of interfacial bonding and atomic vibrations on the formation mechanisms of the PNLs and other structural features at an interface. This makes atomistic modeling essential for further study of the substrate-liquid metal interfaces and the effects of the chemical and dynamical features.

Compared with the homogeneous [29] or heterogeneous metal-metal solid/liquid interfaces [32,63], the substrate-liquid metal interfaces, where a mixture of different types of bonds exists, are more complicated. For the sapphire-Al system, Zhang *et al.* [6] developed a new Al-O interatomic potential based on the framework of the reactive force field (REAXFF). They found in their molecular dynamics (MD) simulations that the interdiffusion of the Al and O atoms at the solid/liquid interface promotes the wetting of liquid Al on the (0001) sapphire surface. They also observed the formation of approximately three PNLs at the (0001) sapphire-liquid Al interface. The (0001) sapphire-liquid Al interfacial structure obtained from the *ab initio* molecular dynamics (AIMD) in Kang *et al.*'s [4] study is similar to the finding of Zhang *et al.* [6], except that the surface termination of the (0001) sapphire in Kang's calculations is Al rich instead of the Al-O mixed configuration reported by Zhang and co-workers [6]. Interestingly, our experiments based on CTR measurement also produced an Al-rich (0001) sapphire surface termination in contact with a two-layer PNL. This experimental finding is consistent with the AIMD results, suggesting that the AIMD simulations can faithfully reproduce the experimentally observed structural features at the (0001) sapphire-liquid Al interface. Therefore, AIMD simulations are utilized in this work to further investigate the effects of bonding and atomic vibrations on the interfacial structures observed in the previous studies of Kang *et al.* [4] and Ma *et al.* [35].

Here we present a comprehensive study of the interfaces of liquid Al with five different (0001) sapphire surfaces (Fig. 1), which includes electronic, structural, thermodynamic, and kinetic analyses. The rest of the paper is arranged as follows. In Sec. II, the initial (0001) sapphire-liquid Al interface model for the AIMD simulations is established, and the parameters employed in this study are explained. In Sec. III A and Sec. III B, the structural features of the interfaces of liquid Al with nonhydroxylated (0001) sapphire and hydroxylated (0001) sapphire surfaces, respectively, are described in detail. In Sec. III C, the interfacial bonding features and the surface dynamical behaviors are analyzed with their influences on the structural features of the interfaces revealed. In Sec. III D, the formation mechanism of the PNLs at the substrate-liquid metal interface is summarized. Conclusions are given in Sec. IV.

II. METHODOLOGY

A. Construction of initial (0001) sapphire-liquid Al interfaces

The crystal structure of sapphire can be described as a conventional hexagonal unit cell with oxygen atoms located at the lattice points that form a hexagonal close-packed structure and aluminum atoms occupying two-thirds of the octahedral interstices of the 3O sublattice. Along the z ([0001]) direction, the atomic layers arrange in the order "–AlOAlAlOAl–," and the subunit cell "AlOAl" can be treated as a basic unit. Five (0001) sapphire surfaces with different surface terminations were prepared first, as shown in Fig. 1. 1Al-terminated [one Al atomic layer terminating the surface of a 1×1 (0001) sapphire substrate, Fig. 1(a)], 2Al-terminated [Fig. 1(b)], O-terminated [Fig. 1(c)], and reconstructed [Fig. 1(d)] (0001) sapphire surfaces are four nonhydroxylated sapphire surfaces; fully hydroxylated (0001) sapphire surface [Fig. 1(e)] was used to represent the sapphire surfaces in a humid environment. It has been well established that the 1Al termination is the most stable nonhydroxylated surface over a broad range of oxygen chemical potentials and temperatures. When the temperature is elevated (~1500 K) [34], a $(\sqrt{31} \times \sqrt{31})R \pm 9^\circ$ surface reconstruction appears and then becomes a stable surface termination, which can be simplified to a 1Al-terminated (0001) sapphire surface with the two outmost oxygen layers removed [Fig. 1(d)] [64,65]. Although the 2Al-terminated and 3O-terminated (0001) sapphire surfaces are not as stable as the 1Al-terminated one, they were also studied to investigate in more detail the influence of surface chemical features on substrate-liquid metal interfacial structures. Compared with the nonhydroxylated (0001) sapphire surfaces, the hydroxylated surfaces are more stable with lower surface energies because of the passivation effect that eliminates the influence of lone pair electrons at the surfaces [53,55,66]. It has been demonstrated that water vapor pressure of 1 Torr (about 133 Pa) is sufficient to fully hydroxylated the (0001) sapphire surface [62], that is, it is quite easy for water molecules to adsorb and dissociate on a nonhydroxylated sapphire surface to form a hydroxylated surface configuration.

It was verified that 5 basic units (15 atomic layers) are large enough to eliminate the interaction between the two (0001) sapphire surfaces in a (0001) sapphire slab model (see Fig. S1 in Supplemental Material [67]). To faithfully reproduce the solid/liquid interfacial structures in the AIMD

simulations, the in-plane size of the interface models should be as large as possible in order to eliminate the influence of the image atom interactions due to periodic boundaries. However, very large supercells will make the AIMD simulations a formidable task because of the enormous computational cost. Consequently, the in-plane size effect is analyzed with the aim of determining the minimum in-plane size ensuring the evolution of the liquid phase to be negligibly affected by the periodic boundaries. 1Al-terminated (0001) sapphire-liquid Al interface model was taken as an example to test the influence of in-plane size on the evolution of the interfacial structure. The six models with different in-plane dimensions (1×1, which is the conventional unit cell of sapphire, 2×2, 3×1, 3×2, 3×3, and 4×4) were calculated. For the 1×1 interface model, simulations broke down even if the MD timestep was decreased to less than 0.1 fs; for the 2×2 interface model, a timestep of 0.1 fs or less was required to ensure the convergence of the total energy during the MD runs; while for the rest of the interface models, a timestep of 1.0 fs was verified to be appropriate for the AIMD simulations. The small timesteps required for the 1×1 and 2×2 supercells are in part attributable to the violent atomic collisions at the periodic boundaries in the x and y directions due to the small in-plane size and relatively large mobility of liquid atoms, which cause the increase of system pressures and temperatures. When the timestep is set to a large value in such small systems, the interface structures may break down due to the sudden increase of system temperatures which causes the simulation to crash.

The solid/liquid interfacial structures based on the 1×1 and 2×2 supercells will not be further analyzed because these results are not reliable due to the obvious influence of the periodic boundaries. Results from the other four supercells (3×1, 3×2, 3×3, 4×4) are shown in Fig. S2 in Supplemental Material [67]. Liquid layers are absent at the 3×1 interface, which is different from the 3×2, 3×3, 4×4 interfaces, where the formation of the PNLs is observed. Therefore, it is concluded that the 3×1 in-plane size is also insufficiently large to eliminate the influence of the periodic boundary conditions. Subsequently, orientational order parameter q_6 (insets in Fig. S3 in Supplemental Material [67]) and 2D structural factor distribution (Fig. S3 in Supplemental Material [67]) are used to compare the in-plane features of the PNLs. It is noteworthy that the in-plane structure of the first prenucleation layer (PNL1) obtained using the 3×2 supercell is obviously more ordered than those in the 3×3 and 4×4 interface models. The anomalous ordering observed in the 3×2 interface system is a manifestation of the size effect caused by the in-plane periodic boundaries. Further increase of the in-plane size from 3×3 to 4×4 shows virtually no influence on both the out-of-plane and in-plane features of the (0001) sapphire-liquid Al interface. Therefore, it was determined that 3×3 is the smallest in-plane size for the (0001) sapphire-liquid Al interface models. All the simulations results presented in the rest of this work have been performed on systems with the 3×3 unit cells in-plane size.

To construct the initial solid/liquid interfaces, the following approach [8] was used: (1) a large solid Al supercell with 32000 atoms was melted and relaxed thermostatically at 950 K using the Large-scale Atomic/Molecular Massive Parallel Simulator [68] (LAMMPS) based on the embedded atom model potential [69]; (2) a random cuboid region that matches the size of the surface models in the x and y directions was extracted from the Al melts obtained in (1) with a 25-Å z-direction length. Additionally, the atomic density of the selected subregion was ensured to be identical to that of the whole liquid system obtained from LAMMPS, which was necessary to maintain the essential features of the Al melts; (3) the liquid region obtained in (2) was combined with the five surface models and then in each solid/liquid interface model, a 15-Å-thick vacuum region was inserted to separate the liquid region and the sapphire substrate in order to avoid the influence of confinement effects [27,70,71].

B. AIMD simulations of the (0001) sapphire-liquid Al interfaces

AIMD simulations were performed using the Vienna *Ab Initio* Simulation Package [72–74] (VASP). In the simulations, the interactions between the electrons and ions were described by the projected-augmented waves [75] method, and the Perdew-Burke-Ernzerhof [76] functional within the generalized gradient approximation (GGA) scheme was employed to approximate the exchange-correlation energy. van der Waals interactions may play an important role at the interface with fully hydroxylated sapphire substrate. To deal with the van der Waals interactions, Cavallotti *et al.* [77] used the local-density approximation (LDA) to approximate the corrected recipe of GGA by the van der Waals interactions, since they found the bonding overestimation for sapphire-metal bonds by the LDA functional was just able to compensates for the missing van der Waals interactions. This is a computationally feasible approach for large systems when only moderate accuracy (for example, in AIMD simulations) is required. Therefore, the LDA was used in the calculation of the fully hydroxylated (0001) sapphire-liquid Al interface. For the five interface models described in Sec. II A, the cutoff energies of the plane waves were all set to 400 eV. The Gaussian smearing method with smearing width of 0.01 eV was used to calculate efficiently and accurately the total energy within each ionic step. Considering the large supercells (around 500 atoms) in all the simulations, only one k point, the Γ point, was used to sample the Brillouin-zone. For the molecular dynamics, canonical (NVT) ensemble with Nosé thermostat was applied to equilibrate the systems, as well as to maintain the system temperature at around 950 K, which is just above the AIMD-based Al melting point [78,79].

C. Analysis of the simulation results

1. Parameters to characterize interfacial structural features

To follow the evolution of the solid/liquid interfaces and describe the layering features at the interfaces, atomic density profiles $\rho(z)$ along the z direction were calculated at all the interfaces studied in this work:

$$\rho(z) = \frac{\langle n_z \rangle}{A_{xy}\Delta z}, \tag{1}$$

where n_z is the number of atoms in a bin between $z - \Delta z/2$ and $z + \Delta z/2$; Δz is the width of the bin (set as 0.1 Å in

this work) and A_{xy} is the cross-sectional area; $\langle\bullet\rangle$ denotes time average. In this work, the evolution of $\rho(z)$ is monitored as simulations proceed for all the five solid/liquid interfaces, which demonstrates that the PNLs form at the four solid/liquid interfaces with nonhydroxylated sapphire substrates while they are absent near the fully hydroxylated sapphire substrate (Sec. III B). In addition, layer widths, δ, of the PNLs, computed using Eq. (2), were used to quantify the degree of out-of-plane order of these quasilayers in the melts.

$$\delta = \left\langle \sqrt{\frac{1}{n}\sum_{a\in \mathrm{PNL}} (z_a - \bar{z})^2} \right\rangle, \tag{2}$$

where a denotes an atom in a PNL; n is the number of atoms in this PNL; z_a indicates the z coordinate of atom a and $\bar{z}$ is the average of the z coordinates of all the atoms in the PNL.

In order to study the in-plane structure of the PNLs, orientational order parameter q_m [80] and 2D structural factor distribution $S(\mathbf{q})$ were calculated. q_m is calculated as follows:

$$q_m = \left\langle \frac{\sum_{i,j,k} \cos[m\theta_{xy}(i,j,k)]}{N_{\cos}} \right\rangle, \tag{3}$$

where i, j, and k are three atoms within the studied PNL with atoms j and k being the nearest neighbors of atom I; $\theta(i,j,k)$ is the angle between $\mathbf{r}_{ij}$ and $\mathbf{r}_{ik}$, and $\theta_{xy}(i,j,k)$ is the angle $\theta(i,j,k)$ projected onto the xy plane; $N_{\cos}$ is the number of $\cos(\bullet)$ to be added. In this work, q_4 and q_6 were calculated, which are effective at distinguishing 2D structures with fourfold and sixfold symmetries from a disordered bulk liquid phase, respectively [80]. $S(\mathbf{q})$ was calculated according to the formula

$$S(\mathbf{q}) = \frac{1}{n}\left\langle \sum_{a=1}^{N}\sum_{b=1}^{N} e^{-i\bullet\mathbf{q}\bullet(\mathbf{r}_a - \mathbf{r}_b)} \right\rangle, \tag{4}$$

where $\mathbf{q}$ denotes the scattering vector, which is a vector in the reciprocal space; i is the imaginary unit; N is the number of atoms in the system; $\mathbf{r}_a$ and $\mathbf{r}_b$ are the positions of atoms a and b, respectively.

2. Analysis of the diffusion and vibration behaviors at interfaces

Dynamical properties of interfaces were quantified by calculating the diffusion coefficient D and the phonon density of states (pDOS) $\Gamma(\nu)$. D was obtained from the slope of the mean-square displacement (MSD) [80]:

$$D = \frac{1}{6}\frac{d}{dt}\sum_{a=1}^{N}\langle|\mathbf{r}_a(t) - \mathbf{r}_a(t_0)|^2\rangle, \tag{5}$$

where N is the number of atoms in a region where D is calculated and a is an atom in this region; t_0 is the time origin; the brackets $\langle\bullet\rangle$ denotes the average over t_0, and in this work this averaging was done over 1000 t_0 for the studied interfaces. $\Gamma(\nu)$ was determined from the Fourier transform of the normalized velocity autocorrelation function $C(t)$ [81,82]

$$C(t) = \left\langle \frac{\sum_{a=1}^{N}\mathbf{v}_a(t)\cdot\mathbf{v}_a(t_0)}{\sum_{a=1}^{N}\mathbf{v}_a(t_0)\cdot\mathbf{v}_a(t_0)} \right\rangle, \tag{6}$$

$$\Gamma(\nu) = 12N\int_0^{\infty} C(t)\cos(2\pi\nu t)dt, \tag{7}$$

where $\mathbf{v}_a(t)$ is the velocity of atom a at time t, and t_0 is the time origin; the brackets $\langle\bullet\rangle$ are the average over t_0 which was done over 1000 different uncorrelated t_0's; ν is the vibration frequency. Equation (7) represents the Fourier transform of $C(t)$. In our calculations, the upper limit of the integral in Eq. (7) is replaced by 20.0 ps which was tested to be large enough to ensure a converged $\Gamma(\nu)$ in each calculation.

3. Electronic structure analysis

The electronic structures of sapphire surfaces and sapphire-liquid Al interfaces were analyzed qualitatively and quantitatively through the charge-density distribution and Bader charge, respectively. In addition, the electron localization function (ELF) [54] was employed to study the interfacial electronic features. The ELF quantifies the "degree of localization" of electrons via analysis based on the Pauli principle [83]. It is easy to distinguish the spatial distribution of localized bonds, e.g., covalent bonds, whose ELF value is close to 1.0, from the metallic bonds with the ELF value of 0.5. Therefore, the interfacial bonding features are intuitively and efficiently presented by the ELF analysis.

III. RESULTS AND DISCUSSION

A. Structural features of the prenucleation layers at the nonhydroxylated (0001) sapphire-liquid Al interfaces

After it is brought in contact with the nonhydroxylated (0001) sapphire surfaces, liquid Al becomes locally ordered and forms partially ordered atomic layers at the interface along the direction normal to the surfaces (the out-of-plane direction). These liquid layers are termed PNLs following our previous work [35], due to the fact that they form above T_{m} of Al and play an important role in the heterogeneous nucleation behaviors of crystalline Al. The formation processes of the four interfaces with nonhydroxylated (0001) sapphire surfaces are analyzed by monitoring the evolution of the atomic density profiles $\rho(z)$ (Fig. S4 in Supplemental Material [67]) and the PNL layer widths δ (Fig. S5 in Supplemental Material [67]). It is found that the structural features of the PNLs at these four interfaces are virtually unchanged after 20 ps. Thus, the interfacial structures obtained after 20 ps are considered as the equilibrated structures. Although the formation kinetics of the PNLs adjacent to the four nonhydroxylated (0001) sapphire substrates show differences (Fig. S5 in Supplemental Material [67]), their equilibrated interfacial structures are essentially the same, as shown in Fig. 2. In fact, this is expected since Al atoms at the interfaces are expected to move freely between the substrate surface and the liquid and thus irrespective of the number of initial Al atoms at the substrate surface, the final interfacial structure will contain the same number of Al atoms in the interfacial layers. Therefore, in the following description, the equilibrated interfacial structure calculated using the O-terminated sapphire substrate is used to represent the nonhydroxylated (0001) sapphire-liquid Al interfacial structure. Figure 3(b) depicts a typical snapshot showing the atomic arrangement at the equilibrated nonhydroxylated (0001) sapphire-liquid Al interfaces, which is compared with the unevolved interface with the O-terminated sapphire as the substrate [Fig. 3(a)]. The comparison of Figs. 3(a) and 3(b)

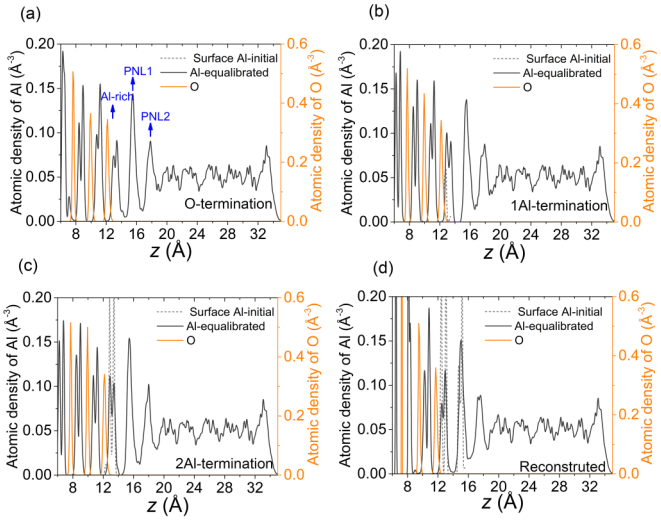

FIG. 2. Atomic density profiles along z direction at the equilibrated interfaces of liquid Al with (a) (0001) O-terminated sapphire surface, (b) (0001) 1Al-terminated sapphire surface, (c) (0001) 2Al-terminated sapphire surface, and (d) Reconstructed (0001) sapphire surface, respectively. Surface Al atoms in the initial interface models are depicted using dotted lines in each panel. Typical structural features of the equilibrated nonhydroxylated (0001) sapphire-liquid Al interface, i.e., Al-rich layer, PNL1, and PNL2 are highlighted in (a).

illustrates the prominent features of the equilibrated interfaces of liquid Al with the nonhydroxylated (0001) sapphire surfaces, which are summarized as follows: (1) an Al-rich termination forms no matter which kind of surface is brought into contact with the liquid Al; (2) several PNLs appear with the one closest to the sapphire surface (designated PNL1 hereafter) showing a high degree of out-of-plane order.

It is intriguing to probe the equilibrated liquid Al-nonhydroxylated (0001) sapphire interfacial structures in more detail. From Fig. 2, it can be noticed that from the

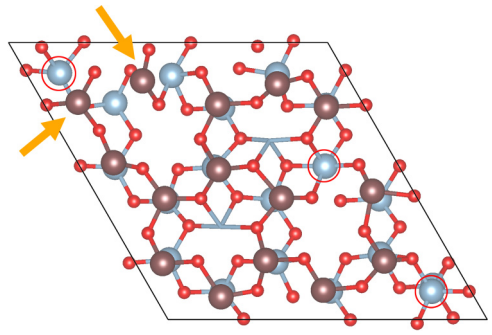

FIG. 4. In-plane atomic arrangement comparison between the Al-rich layer at an equilibrated interface of liquid Al with a (0001) nonhydroxylated sapphire surface (brown spheres) and the 2Al layer at the (0001) 2Al-terminated sapphire surface (gray spheres). The orange arrows point to the two Al atoms in the Al-rich layer that deviate from the atomic sites occupied by the 2Al layer. The red open spheres show the positions of the vacancies in the Al-rich layer compared with the 2Al layer.

perspective of the out-of-plane structure the Al-rich layer is similar to the 2Al layer [depicted by the dotted line in Fig. 2(c)] at the 2Al-terminated (0001) sapphire surface. However, these two structures exhibit apparently different in-plane atomic structural features. In Fig. 4, the Al-rich layer (brown spheres) and the 2Al layer (gray spheres) are stacked together to compare their in-plane atomic arrangements. It is found that the atoms in the Al-rich layer reside on approximately the same sites as those in the 2Al layer, with only a few exceptions (indicated by the orange arrows). Another prominent feature of the Al-rich layer is that the atoms in this layer do not occupy all the atomic sites in the 2Al layer. As shown in Fig. 4, 3 out of 18 sites are not occupied in the Al-rich layer as shown by open red circles in Fig. 4, which is observed for all the equilibrated interfaces with nonhydroxylated sapphire substrates. In other words, the Al-rich layer can be described

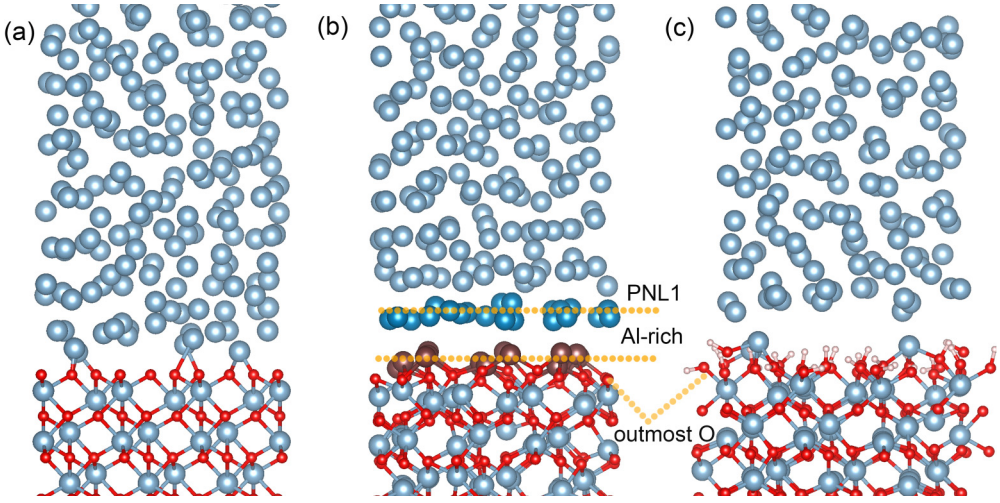

FIG. 3. Atomic arrangements at the initial and evolved (0001) sapphire-liquid Al interfaces. (a) The initial interface model with the O-terminated (0001) sapphire as a substrate; (b) the evolved interfacial structures at 15.0 ps with the (b) nonhydroxylated and (c) hydroxylated (0001) sapphire as substrates, respectively. The large gray spheres are Al atoms, the small red spheres are O atoms, and the smallest white spheres are H atoms. In (b), the Al atoms in the Al-rich layer and in the PNL1 are highlighted as brown and cyan spheres, respectively.

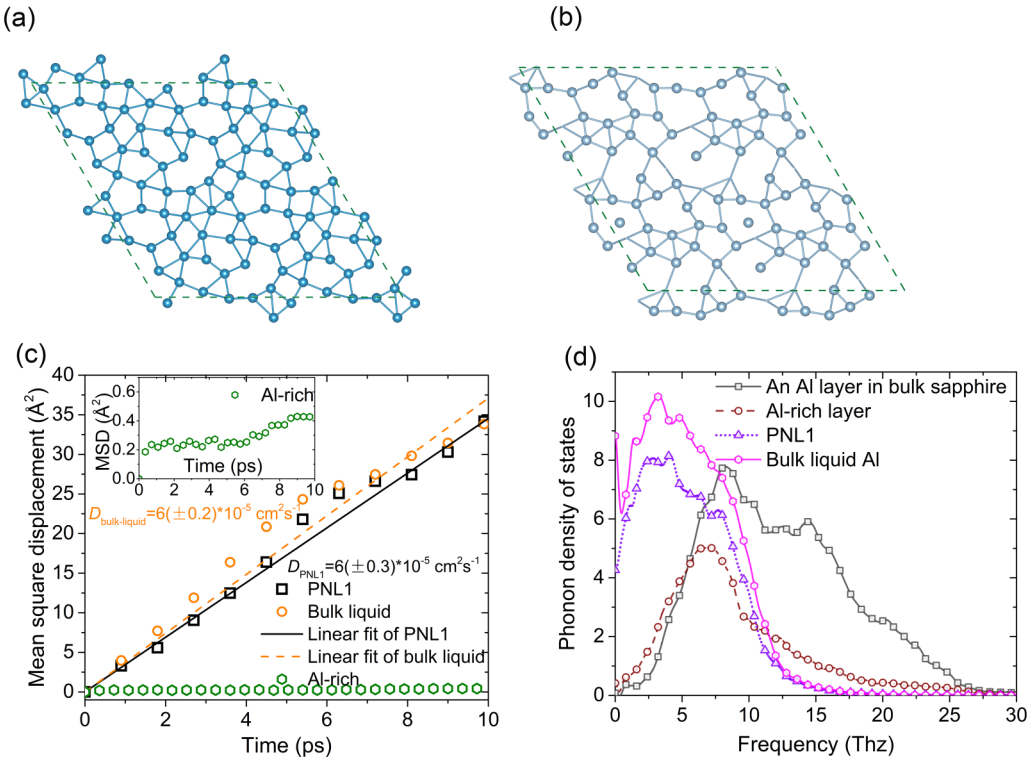

FIG. 5. Comparison of the in-plane structure and dynamical properties in the PNL1 and the bulk liquid Al. (a) and (b) are the in-plane atomic arrangements of the PNL1 and of a layer in the bulk liquid Al (of the same thickness as the PNL1), respectively; (c) mean-square displacements of the atoms in the Al-rich layer, PNL1, and a bulk liquid Al layer, and the calculated diffusion coefficients with estimated errors shown in parentheses; (d) pDOS within different regions at the equilibrated nonhydroxylated sapphire-liquid Al interface which were calculated by combination of Eq. (6) and Eq. (7). The calculated $C(t)$ is shown in Fig. S6 in Supplemental Material [67]. These results were calculated based on the interface with O-terminated (0001) sapphire surface.

as a vacancy-mediated 2Al layer with a vacancy concentration of about 16%. According to Kang *et al.*'s research [4], the Al chemical potential (μ_{Al}) in the 2Al layer is higher than that in the bulk liquid Al, and the formation of vacancies decrease μ_{Al} in the 2Al layer. Therefore, vacancies will continue to form until μ_{Al} in the 2Al layer equals to that in the bulk liquid Al and the 2Al layer is transformed into the Al-rich layer.

Next, the PNLs are studied in detail. From Fig. 2, we can distinguish two PNLs forming above the Al-rich layer. With increasing distance from the sapphire surface, the degree of out-of-plane order of the PNL decreases rapidly. Considering the fact that the in-plane order of a PNL lags behind its out-of-plane order, the second PNL (designated PNL2 hereafter) is not analyzed in this work because its layering feature is difficult to distinguish from the liquid Al structure [Fig. 3(b)]. Therefore, our attention is focused on the PNL1 hereafter. The out-of-plane structural features of a PNL can be directly extracted from its atomic density profiles, and peak width δ is best suited to quantify its degree of out-of-plane order, which can be understood as the z-direction vibration amplitude of the atoms in the PNL. As depicted in Fig. S5 in Supplemental Material [67], the PNL1 at all four interfaces with the nonhydroxylated sapphire substrate form and stabilize within 20.0 ps, and δ of the equilibrated PNL1 is around 0.7 Å. Layer width of the equilibrated PNL1 is small enough to distinguish itself from the Al-rich layer (interplanar distance between the PNL1 and the Al-rich layer is about 2.19 Å) and PNL2 (distance from PNL1 to PNL2 is about 2.30 Å). Therefore, it is reasonable to conclude that the PNL1 is highly ordered in the out-of-plane direction. In Figs. 5(a) and 5(b), the in-plane bonding structures (with cutoff a distance of 3.5 Å) of the PNL1 and of a bulk liquid "layer" (with the same layer width as the PNL1) are displayed, which are extracted from the equilibrated nonhydroxylated interface at the simulation time of 40.0 ps. Compared with the bulk liquid Al, the PNL1 shows a better connected in-plane bonding structure with more hexagonal structures than the bulk liquid layer. The in-plane order of PNL1 is also quantified by the orientational order parameters [80] q_4 and q_6. q_4 and q_6 measured within PNL1 are 0.222 and 0.096, respectively, and measured within a liquid Al slab of the same thickness are 0.067 and -0.043, respectively. According to Davidchack *et al.* [80], q_4 and q_6, which embody the in-plane fourfold and sixfold symmetry, will be close to 1.0 for highly ordered tetrahedral and hexahedral structures, respectively. q_4 and q_6 of PNL1 are both closer to zero rather than 1.0, although q_6 of the PNL1 shows a larger value than that in the bulk liquid. This indicates that the degree of in-plane order is still quite low for the PNL1 at the studied temperature (950 K).

In addition to the structural characteristics analyzed above, the diffusion behavior of the PNL1 is also analyzed to quantify the dynamic behavior of this structure. In Fig. 5(c), MSD

within the PNL1 and of the bulk liquid Al are extracted from the equilibrated AIMD trajectory, from which the diffusion coefficients are calculated correspondingly using Eq. (5). Unlike the solid atomic layers with poor diffusivity [as demonstrated by the MSD curve in Fig. 5(c)], the PNL1 shows a high diffusivity which is at the same level as the bulk liquid Al. The phonon density of states calculated within different regions at an equilibrated (0001) sapphire-liquid Al interface is shown in Fig. 5(d). pDOS of the PNL1 and the bulk liquid Al are similar to each other, with peak frequencies at the same level and obviously lower than those of the bulk sapphire and the Al-rich layer. The above discussion demonstrates that the PNL1 at 950 K is more like the bulk liquid Al instead of a bulk solid atomic layer from the perspective of the dynamical properties, such as the diffusion and atomic vibration behaviors.

The structural features of the Al-rich layer and the PNL1 are separately studied above. When these two structures are treated as the surface termination of the sapphire substrate as a whole, it is interesting to find that this combined termination is almost the same as the reconstructed (0001) sapphire surface, at least from the perspective of the out-of-plane structure, which can be clearly seen in Fig. 2(d). In fact, Shen *et al.* [7,57] have revealed using wetting experiments that the presence of Al shifts the reconstruction transformation temperature of this surface from higher than 1500 K to even less than 1100 K. Therefore, we infer that the formation of the Al-rich layer and the PNL1 is the manifestation of the surface reconstruction after the contact between the nonhydroxylated (0001) sapphire and the liquid Al.

B. Al depletion region and chemical reactions at the hydroxylated (0001) sapphire-liquid Al interfaces

Incorporation of hydroxyls at the (0001) sapphire surface changes its chemical activity, nearly isolating the sapphire surface from the source of electrons provided by the liquid Al. In this section, the structural features and evolution behavior of the fully hydroxylated (0001) sapphire-liquid Al interface are studied in detail and compared to the nonhydroxylated interfaces in order to determine whether the hydroxyls at the interface could influence the structural evolution at the interfaces. Figure 6 shows the atomic density profiles at 40 ps (averaged during the last 5 ps) for the fully hydroxylated interface (the evolution of atomic density profiles at this interface is shown in Fig. S7 in Supplemental Material [67]). Compared to the nonhydroxylated case (see Fig. 2), two key differences are observed: (1) the Al-rich layer is replaced by the Al-depleted region, with the average Al atomic density of less than half of that in the Al-rich layer; (2) there are no PNLs adjacent to the hydroxylated sapphire substrate. The Al-depletion region is a manifestation of the weak substrate-liquid interaction due to the presence of the interfacial hydroxyls. Depicted in Fig. 7 are the magnified atomic density profiles at the interface region, and the evolution of oxygen and hydrogen atoms is emphasized. Within the first 10 ps, atomic density profiles of both oxygen and hydrogen atoms show little change; while after about 20 ps, the oxygen and hydrogen atomic densities are no longer zero at the z range from ~14 to ~15.5 Å. This means that some of the surface hydrogen and oxygen atoms leave the sapphire substrate and diffuse into liquid Al. The

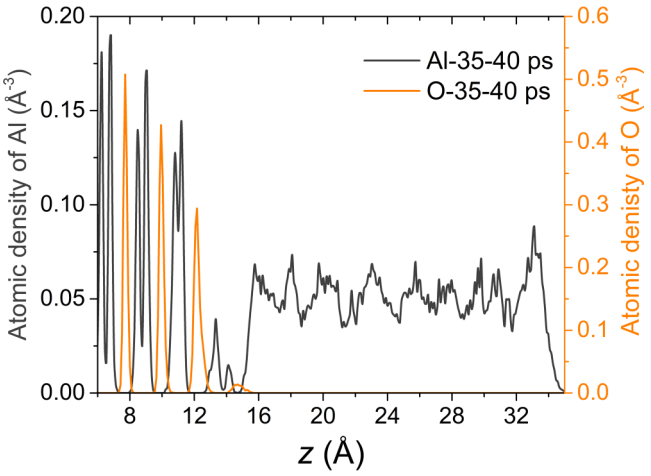

FIG. 6. Atomic density profiles of Al and O atoms along z direction at the fully hydroxylated (0001) sapphire-liquid Al interface. The density profiles are extracted by averaging the interfacial atomic configurations from 35.0 to 40.0 ps. The profile of surface hydrogens is not presented.

dissolution of surface hydroxyls is well established according to the following chemical reaction [84]:

$$2\mathrm{OH}^- + \left(\frac{2}{n}\right)\mathrm{M}^0 \rightarrow 2\mathrm{O}^{2-} + \mathrm{H}_2 + \left(\frac{2}{n}\right)\mathrm{M}^{n+}, \qquad (8)$$

where M denotes a metallic adsorbate that is in contact with the hydroxyls, and in this work, it is aluminum.

To shed light on the possible reaction pathways at the hydroxylated (0001) sapphire-liquid Al interface, the nearest-neighbor pair-distribution functions $P_{\mathrm{A\text{-}B}}(r)$ are calculated at these interfaces.

$$P_{\mathrm{A\text{-}B}}(r) = \left\langle \frac{N_{\mathrm{A\text{-}B}}(r-\Delta r/2, r+\Delta r/2)}{N_{\mathrm{A\text{-}B}}(\mathrm{total})} \right\rangle. \qquad (9)$$

In the above formula, r denotes the length of a nearest-neighbor pair; $N_{\mathrm{A\text{-}B}}(\mathrm{total})$ is the total number of nearest-neighbor pairs between element A and element B; $N_{\mathrm{A\text{-}B}}(r-\Delta r/2, r+\Delta r/2)$ is the number of A-B nearest-neighbor pairs with pair distance between $r-\Delta r/2$ and $r+\Delta r/2$ and Δr is set as 0.1 Å. In Fig. 8(a), it is observed that a peak for $\mathrm{P_{H\text{-}H}}$ emerges at approximately 0.75 Å, which implies the formation of hydrogen molecules (H–H bond length in hydrogen molecule is 0.74 Å). Meanwhile, the primary peak of $P_{\mathrm{O\text{-}H}}(r)$ and $P_{\mathrm{O\text{-}Al}}(r)$ shifts to a larger and a smaller value, respectively, suggesting weakening of the interfacial O–H bonds and strengthening of the interfacial O–Al bonds. These weakened O–H bonds are ready to break down and release the hydrogen atoms to form the hydrogen molecules as mentioned above; oxygen atoms with unpaired electrons are also produced as a result of the O–H bond breaking, which will attract the Al atoms to form strong O–Al bonds. The above discussion based on Fig. 8 supports the reaction mechanism in Eq. (7). However, the outward diffusion of the surface oxygen atoms shown in Fig. 7(b) is not accounted for through Eq. (7). In fact, it is observed in our simulations that some of the surface oxygen atoms tend to break away from the bulk sapphire and dissolve into the liquid Al along with the dissolution of surface

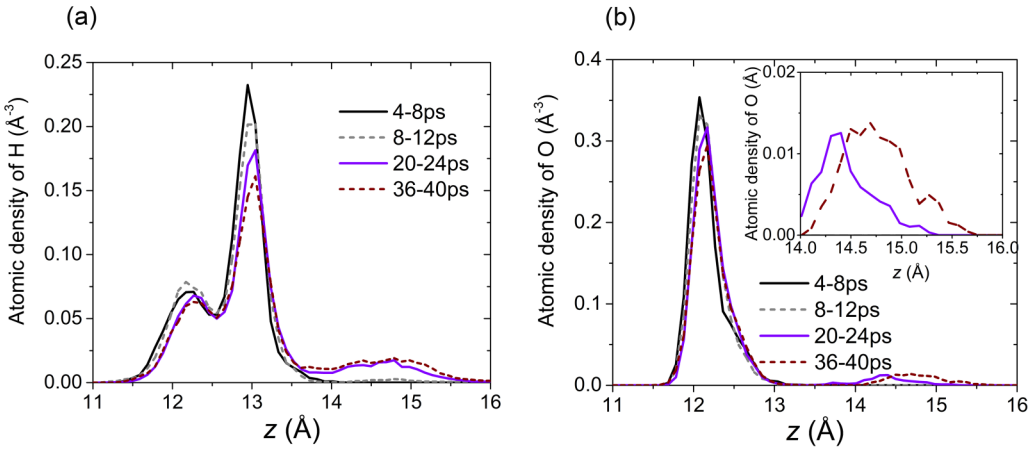

FIG. 7. Evolution of z-direction atomic density profiles of H (a) and O (b) atoms at the fully hydroxylated (0001) sapphire-liquid Al interface. Outward diffusion of H and O atoms from the sapphire substrate into the liquid Al is found after 20 ps, which is manifested by the appearance of density peaks between $z = 14$ Å and $z = 15$ Å, magnified in the inset in (b).

hydroxyls. This indicates that the presence of hydroxyls may destabilize the surface oxygen layer of the sapphire substrate compared with the one directly in contact with the liquid Al.

From the above discussion, the features of the fully hydroxylated (0001) sapphire-liquid Al interface are summarized as follows. First, an Al depletion region forms immediately after the contact between sapphire surface and liquid Al, which separates the sapphire substrate from the bulk liquid Al. Then, after ∼20 ps, a small number of the hydroxyls and surface oxygen atoms overcome the energy barrier caused by the sapphire substrate and diffuse into the liquid Al. Although interfacial equilibrium at this interface is not reached in our AIMD simulations due to the computational capacity limitation, it is reasonable to predict that the dissolution of the surface hydroxyls and diffusion of the surface oxygen atoms into the liquid Al will prevail during the following interaction at the interface. For now, we focus our attention on the structural differences at the interfaces of liquid Al and differently terminated (0001) sapphire surfaces and to the underlying reasons causing such differences.

C. Electronic structures and dynamical behaviors of the (0001) sapphire-liquid Al interfaces

A question arises from the comparison of the interfacial structural features between the nonhydroxylated (Sec. III A) and hydroxylated (Sec. III B) (0001) sapphire-liquid Al interfaces: Why are the interfacial structures of liquid Al with nonhydroxylated and hydroxylated (0001) sapphire substrates different? To answer this question, it is necessary to first study the electronic nature of the five different sapphire surfaces in detail. Shown in Fig. 9 are the charge-density distributions (yellow and green isosurfaces indicate valence electron density values of 0.03 and 0.3 e bohrs^{-3}, respectively) at the (0001) sapphire surfaces, which qualitatively depict the electronic features of these surfaces. Surface dipoles form due to the accumulation and depletion of valence electrons at the O-terminated [Fig. 9(a)] and 2Al-terminated [Fig. 9(c)], reconstructed [Fig. 9(d)] sapphire surfaces, respectively, indicating that these three surfaces are unstable. Incorporation of one extra Al layer or H layer onto the O-terminated sapphire surface leads to the 1Al-terminated [Fig. 9(b)] or the fully

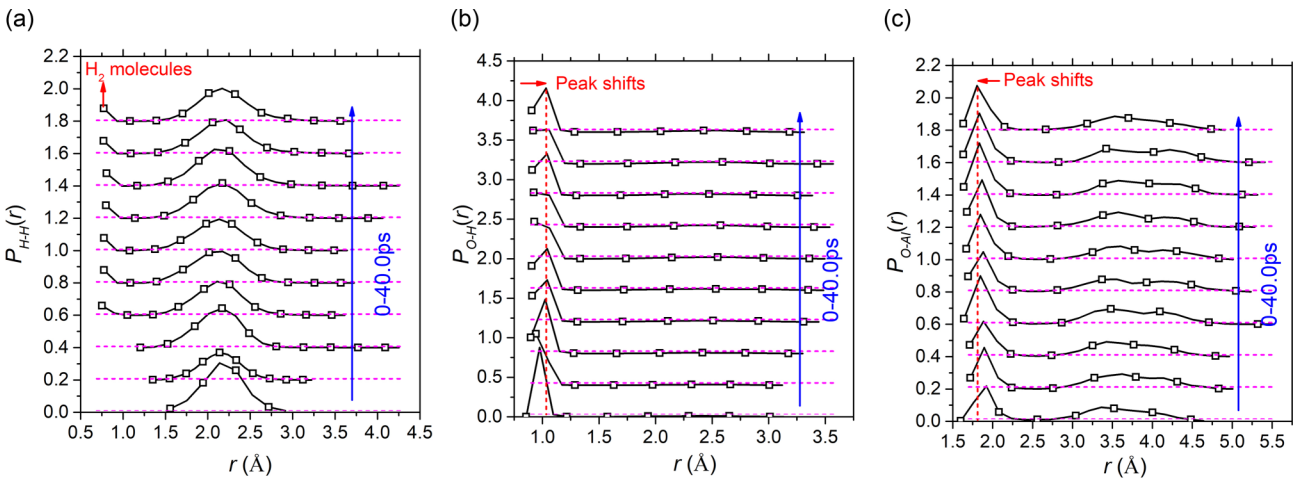

FIG. 8. Evolution of the nearest-neighbor pair-distribution functions of (a) H-H pair, (b) O-H pair, and (c) O-Al pair at the fully hydroxylated (0001) sapphire-liquid Al interface from 0 to 40.0 ps.

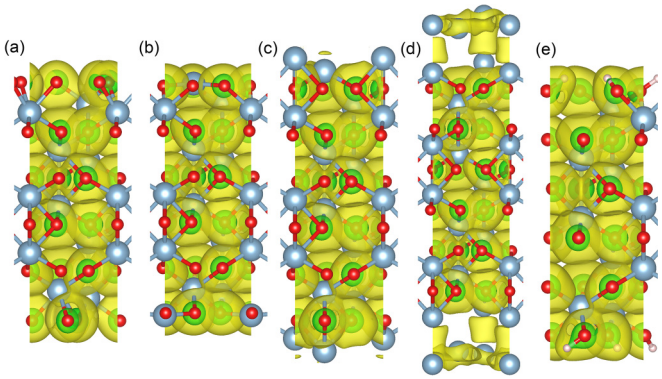

FIG. 9. Valence electron density at the five (0001) sapphire surfaces with different terminations: (a) O termination, (b) 1Al termination, (c) 2Al termination, (d) reconstructed surface, and (e) fully hydroxylated surface. Valence electron density isosurfaces at 0.3 and 0.03 e bohrs^{-3} are shown in green and yellow, respectively. The large gray spheres are Al atoms, the small red spheres are O atoms, and the smallest white spheres in (e) are H atoms.

hydroxylated [Fig. 9(e)] sapphire surfaces, respectively, which effectively eliminates the surface dipole. Therefore, the 1Al-terminated and fully hydroxylated sapphire surfaces are more stable. Next, quantitative analysis of the surface electronic features is conducted using the Bader charge method. In Fig. 10, the calculated Bader charge distributions at the five studied sapphire surfaces are shown. Al and O atoms in the bulk sapphire are shown to be +2.48 e and −1.66 e charged, respectively, indicating that Al and O atoms in the bulk sapphire are bonded by a mixture of ionic and covalent bonds. The stability of a surface can be judged by the charge states of the surface atoms compared with their bulk counterparts: the more similar to the charges to those in the bulk, the more stable the surface. Accordingly, the O-terminated, 2Al-terminated, and reconstructed [Figs. 10(a), 10(c), and 10(d)] surfaces are unstable because the Bader charges of the surface oxygen atoms (∼–0.88 e) and the surface Al atoms (∼+1.5 e at the 2Al-terminated surface and ranging from ∼+1.18 to ∼+0.15 e at the reconstructed surface) for these three surfaces are substantially different from the charges of these atoms in the bulk sapphire. This conclusion is consistent with the observation of surface dipoles in Fig. 9. At the 1Al-terminated surface, shown in Fig. 10(a), Bader charges of both the surface Al and O atoms are close to those in the bulk sapphire, so this surface is more stable. Similarly, the presence of surface hydroxyls narrows the difference of Bader charge for oxygen atoms at the sapphire surface and in the bulk, which confirms the stabilizing effect of the surface hydroxyls at the sapphire surface.

From the above qualitative and quantitative electronic analysis it is found that the 1Al-terminated and full hydroxylated sapphire surfaces are the most stable surfaces among the five studied surfaces, which is consistent with the previous findings from the perspective of interfacial thermodynamics [34,55,64]. The presence of liquid Al changes the stable surface terminations of (0001) sapphire substrate. Al chemical potential, μ_{Al}, is calculated using the approach proposed by Kang *et al.* [4] In the bulk sapphire it is calculated to be −8.522 eV which is lower than the bulk liquid Al ($\mu_{\mathrm{Al}} =$ −4.287eV). Meanwhile, Bader charge of Al in the bulk sapphire is ∼+2.5 e and around zero in the liquid Al (as shown in Fig. 11). Normally, chemical potential and Bader charge of the same element are intimately related [42], which means that in the sapphire-Al interface systems, the ∼+2.5 e charged Al ions show lower chemical potential than the neutral Al atoms. Accordingly, to minimize interfacial energy, it is expected that some of the liquid Al atoms may transfer their electrons to the sapphire substrate and become Al ions with positive charges. According to the above analysis (Fig. 10), surface Al ions (with ∼+2.42 e) at the 1Al-terminated (0001) sapphire surface is a much better electron acceptor than the H ions (with ∼+0.64 e) at the fully hydroxylated (0001) sapphire surface. This indicates that transfer of electrons from the liquid Al to the 1Al-terminated sapphire surface is much more significant than to the fully hydroxylated sapphire surface. Accompanying the electron transfer, the oxidized Al ions adsorb onto the sapphire substrate, which changes the initial sapphire surface termination. Similar to the electron transfer, many more newly oxidized Al ions are expected to adsorb onto the 1Al-terminated sapphire surface compared to the fully hydroxylated one. Bader charge distributions extracted from the equilibrated nonhydroxylated (0001) sapphire-liquid Al interface and the fully hydroxylated (0001) sapphire-liquid Al interface at 15.0 ps are shown in Fig. 11. It can be seen that the Al Bader charge transition from ∼+2.5 to ∼ 0 e is found at the surface Al layers of the sapphire substrates with the transition

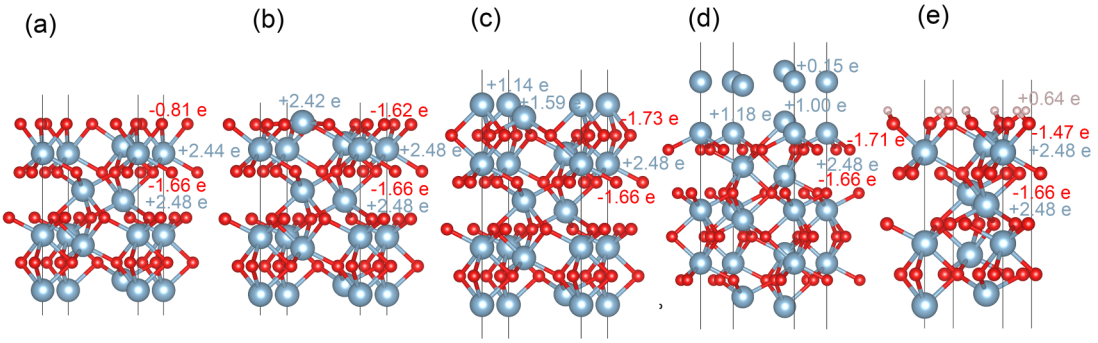

FIG. 10. Bader charge distributions at (a) O-terminated, (b) 1Al-terminated, (c) 2Al-terminated, (d) reconstructed, and (e) fully hydroxylated (0001) sapphire surface, respectively. The large gray spheres are Al atoms, the small red spheres are O atoms, and the smallest white spheres are H atoms. The number near an atom is its Bader charge and "e" is the electron charge.

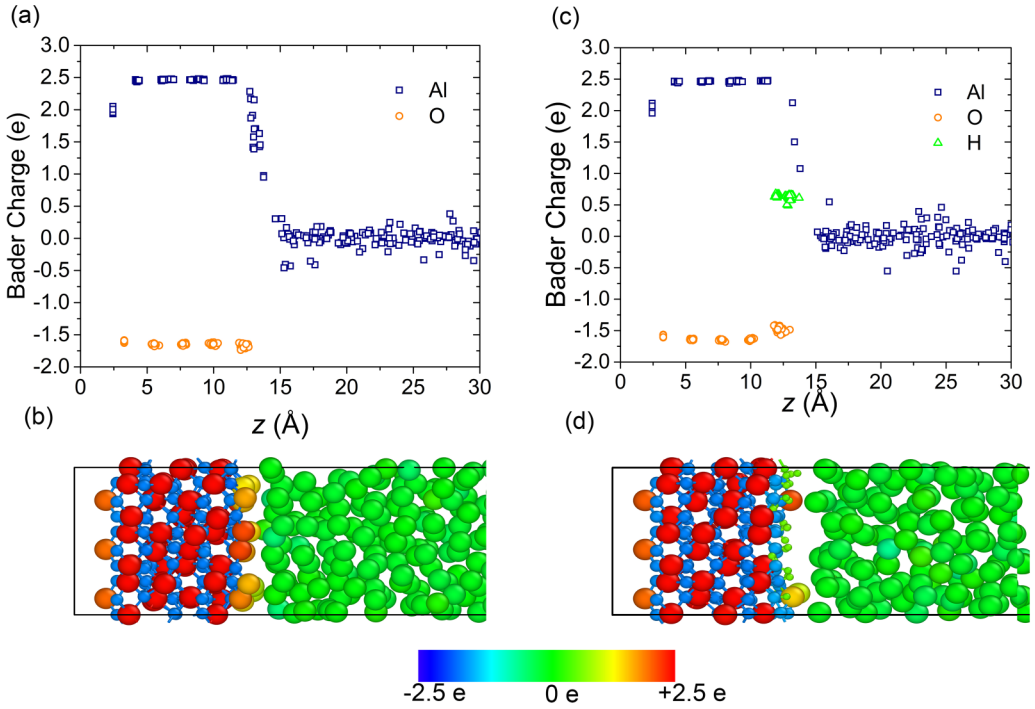

FIG. 11. Bader charge distributions across the interfaces at the interface of liquid Al with the (a), (b) nonhydroxylated (0001) sapphire surface and (c), (d) the fully hydroxylated (0001) sapphire surface. (a), (c) Bader charge profiles of Al, O, and H atoms along z direction across the interfaces; (b), (d) interfacial Bader charge distributions at the above two interfaces. In (b) and (d), the color is based on the calculated Bader charge for each atom. The largest spheres are the Al atoms, the smallest ones are the H atoms, and those of medium size are the O atoms.

at the nonhydroxylated sapphire surface much "smoother" than that at the fully hydroxylated one. In fact, as mentioned above, the transition of Al Bader charge across the interface is a way to minimize the interfacial energy. When liquid Al is brought into contact with the 1Al-terminated sapphire surface, a large gap in the Bader charge between the substrate surface Al ions and the neutral Al atoms in the liquid exists. This prompts the oxidization of the liquid Al atoms near the substrate which greatly decreases the interfacial energy. With more liquid Al atoms oxidized, the Bader charge gap between the Al ions of sapphire surface and the liquid Al gradually narrows, resulting in the decrease of the driving force for further oxidization. Equilibrium is reached when the Bader charge gap is so small that no more liquid Al can be oxidized, as shown in Fig. 11(a), when the interfacial energy should also reach the minimum. This is why the Al-rich layer instead of the 1Al layer becomes the sapphire surface termination in the presence of liquid Al. Near the fully hydroxylated sapphire surface, the hydrogens inhibit the electron transfer, which is why few liquid Al atoms are oxidized and adsorb to the sapphire surface. Consequently, the Al-rich layer is not formed at the fully hydroxylated sapphire surface when the liquid Al is present.

Different bonding features are expected at the interfaces of liquid Al with the Al-rich terminated and the fully hydroxylated (0001) sapphire surfaces. Electron localization function [54,83] is employed to identify the bonding features at the interfaces. To obtain the ELF distribution at a solid/liquid interface, in this work we spatially averaged the ELF distributions extracted from 20 configurations during the last 1 ps of the simulation. In Figs. 12(a) and 12(c), ELF = 0.8 isosurfaces are used to visualize the spatial distribution of covalent bonds at the solid/liquid interfaces with the nonhydroxylated and the fully hydroxylated sapphire surfaces. At the nonhydroxylated interface [Fig. 12(a)], it is interesting to find that ELF is similar to that of the reconstructed sapphire surface [Fig. 12(b)], especially in the region between the

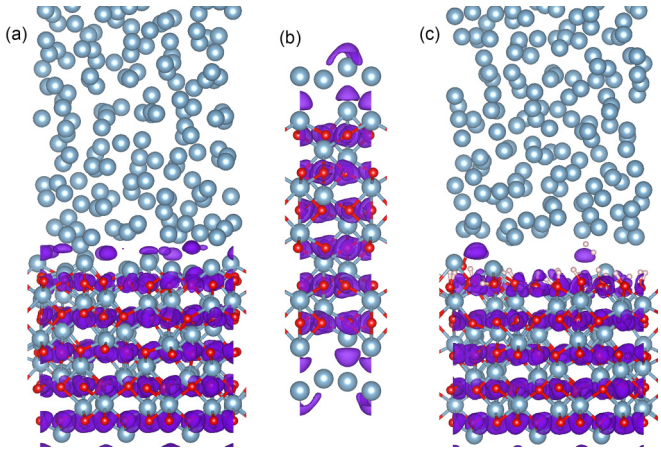

FIG. 12. Electron localization function of the reconstructed (0001) sapphire surface and the evolved (0001) sapphire-liquid Al interfaces. (a) and (c) are calculated based on the equilibrated nonhydroxylated sapphire-liquid Al interface and the fully hydroxylated (0001) sapphire-liquid Al interface, respectively. (b) is calculated using the reconstructed sapphire surface. The violet surfaces are the isosurface of ELF = 0.8, which effectively describes the distribution of localized bonds at these interfaces.

Al-rich layer and the PNL1 where quite a large part of the space is occupied by localized electrons. This suggests that covalent bonds exist between these two Al atomic layers. These covalent bonds play an extremely important role for the formation of the PNLs, stabilizing the PNLs (at least PNL1) at the temperature higher than the liquidus temperature. At the fully hydroxylated interface [Fig. 12(c)], only a small portion of the space between the sapphire surface and the liquid Al is occupied by localized electrons, which are all located around oxygen atoms that diffuse out of the sapphire surface. Such an ELF distribution indicates that covalent bonds are not formed between the substrate and the liquid Al at the fully hydroxylated interface. The absence of chemical bonds makes the substrate-liquid Al attraction at such an interface much weaker than those at the interfaces with nonhydroxylated sapphire surfaces, which should be an important reason causing the absence of the PNLs at near the fully hydroxylated sapphire surface.

In addition to the bonding features, the surface dynamical behavior is analyzed for the different substrates. Here, we focus on the surface dynamics of the substrates that are in contact with liquid Al, and the nonhydroxylated sapphire substrate refers to the sapphire substrate terminated by the Al-rich layer. As mentioned in Sec. III A, diffusion of the Al atoms in the Al-rich layer of the equilibrated nonhydroxylated sapphire substrate is negligible, and the Al atoms that are in direct contact with liquid Al are only observed to vibrate around their equilibrium positions during the simulation period. In contrast, some of the atoms in the outmost O and H layers of the fully hydroxylated sapphire substrate are observed to diffuse out of the layer into the liquid Al after 20.0 ps. The above comparison implies a higher surface atoms mobility of the fully hydroxylated sapphire substrate compared to the nonhydroxylated ones.

Next, the surface dynamical behaviors of these two types of substrates are compared in detail. pDOS of the outmost O layers at the nonhydroxylated and fully hydroxylated interfaces are also compared (Fig. 13). In this figure, lower peak frequency is observed for the O atoms at the fully hydroxylated sapphire substrate compared to that at the nonhydroxylated sapphire substrate. This suggests that the presence of surface hydroxyls considerably weakens the bonding strength of the O atoms to the bulk sapphire, which explains why some of the O atoms at the hydroxylated sapphire surface diffuse into the liquid Al. Meanwhile, it can be inferred from the weakened bonding between the outmost O layer and the bulk sapphire that the vibration amplitude of this O layer should be larger than that in the nonhydroxylated sapphire surface. This conjecture is confirmed in Fig. 14, which depicts the trajectories of the outmost O atoms from 15.0 to 25.0 ps at the nonhydroxylated and hydroxylated sapphire substrates. The red dashed lines in Fig. 14 indicate the vibration amplitudes of the studied O atoms, and the blue dashed line in Fig. 14 (b) shows the diffusion distance of the O atoms during the period of 15.0 to 25.0 ps at the fully hydroxylated sapphire substrate. The vibration amplitude of the outmost O layer at the nonhydroxylated sapphire substrate is found to be 0.7 Å, less than half of that at the fully hydroxylated sapphire substrate (1.6 Å). From the above analysis, we find that the outmost O layer at the fully hydroxylated sapphire substrate shows higher mobility and larger vibration amplitude than that at the nonhydroxylated sapphire substrate.

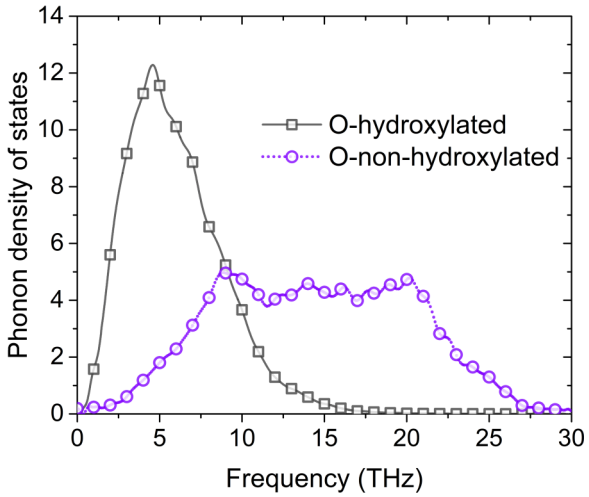

FIG. 13. pDOS of the outmost O layers of the sapphire substrate at the interfaces of liquid Al with nonhydroxylated and hydroxylated (0001) sapphire surfaces. These results were computed by using Eqs. (6) and (7), and the calculated velocity autocorrelation functions are shown in Fig. S8 in Supplemental Material [67].

We now compare the dynamical behaviors of the outmost layers of these two sapphire substrates, i.e., the Al-rich layer for the nonhydroxylated sapphire substrate and the H layer for the fully hydroxylated sapphire substrate. Figure 15 shows the atomic trajectories from 15.0 to 25.0 ps of the atoms in these two layers. Obviously, the mobility of the H layer is much better than the Al-rich layer, and as for the vibration amplitude, both the out-of-plane [Figs. 15(a) and 15(c)] and in-plane [Figs. 15(b) and 15(d)] vibration amplitudes of the H atoms are larger than the Al atoms in the Al-rich layer. In summary, the surface dynamical behavior of the nonhydroxylated sapphire substrate is characterized by the poorer mobility and smaller vibration amplitude compared to the fully hydroxylated sapphire substrate. Fast diffusion and large vibration amplitude of the substrate surface atoms render a rapidly changing potential field which determines the forces acting on the liquid Al atoms adjacent to the substrate. Under such conditions, the formation of PNLs is suppressed since

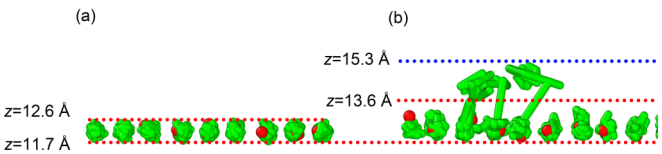

FIG. 14. Atomic trajectories of the oxygen atoms in the outmost oxygen layers of the (0001) sapphire substrates. (a) and (b) are extracted from the equilibrated nonhydroxylated (0001) sapphire-liquid Al interface and the fully hydroxylated (0001) sapphire-liquid Al interface, respectively. The trajectories are extracted during the period from 15.0 to 25.0 ps. The dashed red lines show the out-of-plane vibration amplitude of these oxygen atoms, and the dashed blue line indicates the diffusion distance of the oxygen atoms at the fully hydroxylated sapphire surface.

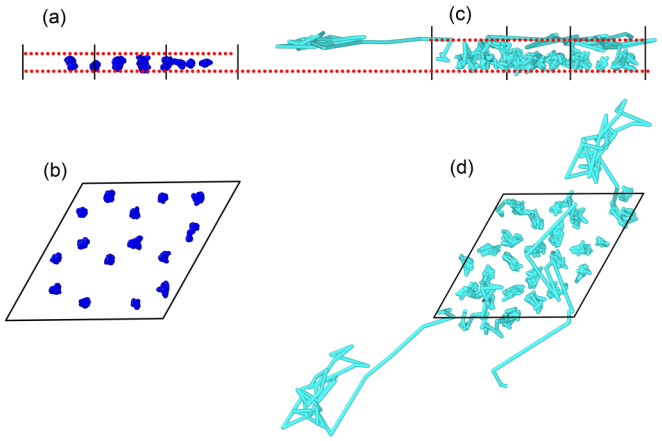

FIG. 15. Atomic trajectories of atoms (a), (b) in the Al-rich layer at the equilibrated nonhydroxylated (0001) sapphire-liquid Al interface and (c), (d) in the outmost hydrogen layer at the fully hydroxylated (0001) sapphire-liquid Al interface. (a) and (c) are the side views of the atomic trajectories; (b) and (d) are the top views of the atomic trajectories. The dashed red lines show the out-of-plane vibration amplitude of the Al and H atoms in (a) and (c), respectively.

the potential wells where the liquid Al atoms aggregate to form the PNLs are not localized due to the large vibrations or diffusion of the substrate surface atoms.

It is worth noting that, except for the bonding features and dynamical behavior discussed above, the lattice mismatch between the substrate and the PNLs is another important factor influencing the formation of the interfacial structure [12,45,48]. Since the lattice mismatches at all the studied interfaces in this work are the same, the influence of lattice mismatch will not be discussed here.

D. Formation mechanism of the PNLs at the substrate-liquid metal interfaces

As the first step to unveil the formation mechanism of the PNLs at the (0001) sapphire-liquid Al interfaces, force distributions $F_{Sz}(x, y, z)$ above the five studied (0001) sapphire surfaces are calculated, as shown in Fig. 16. $F_{Sz}(x, y, z)$ denotes the z component of a probe Al atom at position (x, y, z) which is above the sapphire surfaces. In Fig. 16, $z = 0$ is aligned with the outmost atomic layer of one surface, and for clarity the isosurfaces of $F_{Sz}(x, y, z) \leqslant 0.5\,\text{eV Å}$ are not shown except for those with $F_{Sz}(x, y, z) = -1.0\,\text{eV Å}$ and $F_{Sz}(x, y, z) = -2.0\,\text{eV Å}$. A positive $F_{Sz}(x, y, z)$ moves the probe Al atom away from the surface and vice versa. It is interesting to find that with z getting larger, $F_{Sz}(x, y, z)$ above all the nonhydroxylated surfaces decreases from large positive values to around $-2.0\,\text{eV Å}$ before returning back to zero at large z. For this kind of surface force distribution, a surface potential well exists (marked by the yellow arrows in Fig. 16) at the z position where $F_{Sz}(x, y, z)$ first reaches zero, i.e., $F_{Sz}(x, y, z) = 0$ and $\partial F_{Sz}(x, y, z)/\partial z < 0$. Al atoms tend to aggregate around the potential well surfaces and form

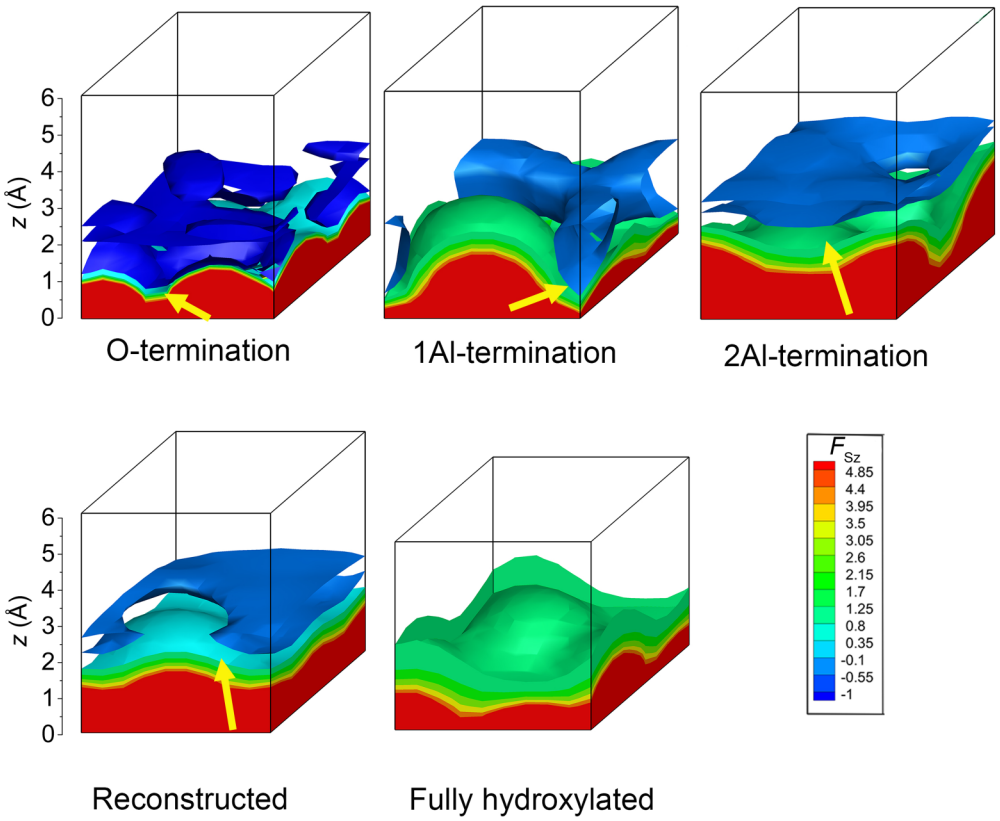

FIG. 16. Surface force distributions F_{Sz} (eV Å^{-3}) above the five different (0001) sapphire surfaces. F_{Sz} is calculated by placing a probe Al atom at position (x, y, z) and extracting the z component of the force imposed on it. $z = 0$ is aligned with the outmost atomic layer of each surface. For clarity $F_{Sz} < 0$ eV Å^{-3} is not shown except for $F_{Sz} = -1.0$ eV Å^{-3} and $F_{Sz} = -2.0$ eV Å^{-3}.

an atomic layer. Therefore, all four nonhydroxylated sapphire surfaces have the potential to induce the formation of an extra Al layer when liquid Al is brought into contact with them. To be specific, above the 3O-terminated (0001) sapphire surface [Fig. 16(a)], the potential well appears approximately in the region $0.7\,\text{Å} < z < 1.5\,\text{Å}$. This is exactly where the Al-rich layer forms when liquid Al is present. Then, above the 1Al-terminated (0001) sapphire surface [Fig. 16(b)], another potential well is found at $z \approx 0.6\,\text{Å}$, where the second sublayer of the Al-rich layer forms. Above the 2Al-terminated sapphire surface [Fig. 16(c)], potential well appears at about $1.6\,\text{Å} < z < 2.5\,\text{Å}$, and coincides with the region where the PNL1 appears at the solid/liquid interface. Finally, above the reconstructed sapphire surface, surface potential well exactly predicts the formation of the PNL2 when it is in contact with liquid Al. In addition to the nonhydroxylated sapphire surfaces, the surface force distribution above the fully hydroxylated sapphire surface was also extracted as shown in Fig. 16(e). Virtually no negative value is found for $F_{\text{Sz}}(x, y, z)$, indicating that there is no surface potential well above this surface. Consequently, Al layers are hard to form above the fully hydroxylated surface. Although the above analysis is based on the surface force distributions, the formation of the Al-rich layer and the PNLs, which are the key structures at the equilibrated nonhydroxylated sapphire-liquid Al interface, and the absence of the PNLs at the fully hydroxylated sapphire-liquid Al interface are correctly predicted. This indicates that by only using the surface force distribution of the substrate, the substrate-liquid metal interfacial structure can be reliably predicted. Also, the above results demonstrate that the manifestation of a substrate-metal interfacial structure is determined by the interaction between the substrate and the metal atoms, i.e., forces imposed on the metal atoms by the substrate. We find that the main difference of surface force distributions between the nonhydroxylated and the fully hydroxylated sapphire surfaces is the magnitude of the attractive forces between the substrate and the metal atoms. Obviously, for the nonhydroxylates sapphire surfaces which impose sufficiently large attractive forces on the Al atoms that are at a certain distance from them, the PNLs are observed to form (Fig. 2), while for the fully hydroxylated sapphire surface, where nearly no attractive force between the substrate and the Al atoms can be detected, no PNL is able to form. Therefore, it is confirmed that the substrate-liquid metal attraction is a key factor determining the structural feature of the interface. As is already well known, the force between two atoms is intrinsically the manifestation of the electronic density distribution or the bonding between them. Accordingly, the substrate-liquid metal attraction reflects the bonding features at the interface. As discussed in Sec. III C, much stronger bonding is observed at the nonhydroxylated sapphire-liquid Al interface compared to the fully hydroxylated sapphire-liquid Al interface, which is the origin of the difference in attractive forces at these interfaces.

Next, we calculated the force profiles $F_{\text{lz}}(z)$ across the sapphire-liquid Al interfaces based on the AIMD simulation results:

$$F_{\text{lz}}(z) = \left\langle \frac{\sum_{z-\Delta z'/2<z_a<z+\Delta z'/2} \tilde{F}_z^a}{n'_z} \right\rangle, \tag{10}$$

where $\tilde{F}_z^a$ is the z component of the force acting on atom a, which is averaged over all the atoms in the region $z - \Delta z'/2 < z_a < z + \Delta z'/2$ ($\Delta z'$ is 0.5 Å in this work); n'_z is the number of atoms in this region. Figure 17 shows the $F_{\text{lz}}(z)$ within the first 2.0 ps for the interfaces with nonhydroxylated and hydroxylated sapphire substrates. Interfacial potential wells (shown by shaded rectangles in Fig. 17), which have the same definition as the surface potential wells, are observed for the interfaces with nonhydroxylated sapphire surface. Interestingly, the interfacial potential wells at each interface correspond exactly to the two interfacial layers, i.e., the Al-rich layer and the PNL1. On the contrary, at the interface with fully hydroxylated sapphire surface [Fig. 17(b)],

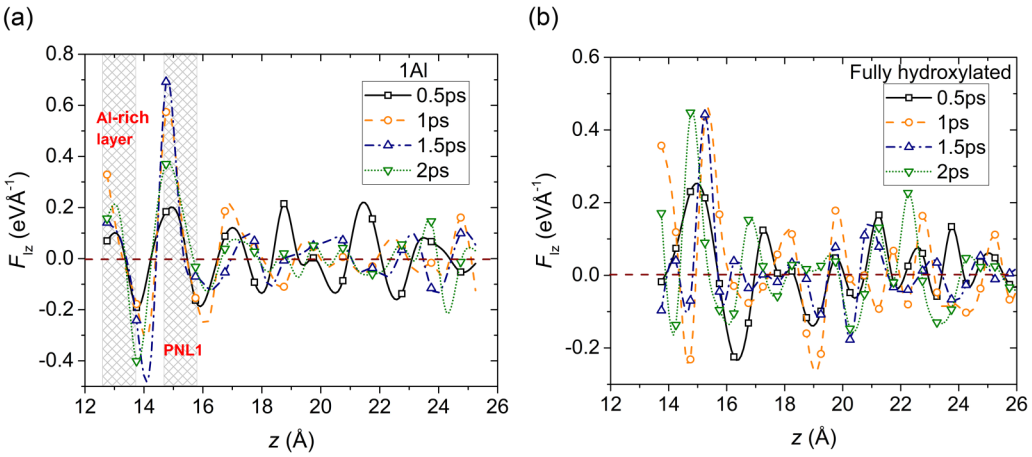

FIG. 17. Interfacial force profiles F_{lz} along z direction at the interfaces of liquid Al with (a) the 1Al-terminated (0001) sapphire substrate [which is a representative of the nonhydroxylated (0001) sapphire-liquid Al interface] and (b) the fully hydroxylated (0001) sapphire substrate. F_{lz} is obtained by averaging the z component of the forces acting on Al atoms in the region $[z - \Delta z'/2, z + \Delta z'/2]$, where $\Delta z'$ is the bin size, set at 0.5 Å. The horizontal axis in (a) and (b) starts from $z = 12\,\text{Å}$, which is the position of the outmost O layer of the sapphire substrate. Interfacial potential wells are shown by the shaded rectangles, which are regions where Al atoms tend to aggregate. They are present at the interface with the nonhydroxylated sapphire surface, but absent near the fully hydroxylated sapphire surface.

no interfacial potential well is observed, which explains why no Al layer forms at this interface. By comparing the surface force distributions in Fig. 16 and the interfacial force profiles in Fig. 17, we find that, although the main structural features of the studied interfaces are correctly predicted from both parameters, a difference still exists in the layering behavior. In Figs. 16(a)–16(d), a layer-by-layer growth of Al layers is observed, which will continue beyond the PNL2 if sufficient Al atoms are supplied. On the other hand, in Fig. 17(a), prominent liquid layering can only be detected at the positions where the Al-rich layer and the PNL1 appear. The above difference is attributed to the different dynamical behaviors of the systems. We note that the surface force distributions in Fig. 16 were calculated at 0 K, and thus the dynamical behaviors of the sapphire substrate and the Al atoms were not considered. The results of the sapphire-liquid Al interfaces were obtained at 950 K, where the dynamical behavior of the substrate surface and the Al atoms would considerably decrease the degree of order of the PNLs, which is the reason why only two PNLs form at the nonhydroxylated sapphire-liquid Al interface.

It is also worth noting that, due to the extremely weak attraction of the fully hydroxylated (0001) sapphire substrate to Al atoms (Fig. 16), the liquid Al atoms adjacent to this substrate are supposed to have structural properties similar to those at the liquid Al surface. However, from Fig. 6, prominent layering of Al atoms at the liquid surface is observed, while no distinguishable layering of Al atoms is detected near the fully hydroxylated sapphire substrate. In fact, termination of a bulk liquid metal phase with a solid or a vacuum stratifies the liquid atoms in the interface or at the surface due to the geometrical confinement mechanism [85]. Accordingly, when liquid Al is brought into contact with the fully hydroxylated sapphire substrate, the Al atoms adjacent to the substrate have the tendency to self-assemble in a more ordered arrangement. However, this inherent tendency is inhibited by the surface dynamical behavior of the substrate, i.e., fast diffusion and vibration with large amplitude of the substrate surface atoms causing a different atomic configuration from the liquid Al surface.

In summary, the formation mechanism of the PNLs at a substrate-liquid metal interface can be described as follows (schematically illustrated in Fig. 18). Liquid metal atoms in contact with a solid substrate show smaller coordination number (CN) than those in the bulk liquid. Increase of the CN of the interfacial liquid metal atoms will decrease the interfacial energy, which manifests itself as a spontaneous layering of these atoms. Bonding between the substrate and the adjacent liquid metal atoms enhances the layering, and the stronger the interfacial bonding the more ordered the PNLs in the interface. Surface dynamical behavior of the substrate inhibits the layering: the faster diffusion or larger vibration amplitude of the surface atoms, the less ordered the PNLs are. In addition, the lattice mismatch between the substrate and the layered structures of the liquid metal, which quantifies the interfacial strain energy, also impedes the liquid layering. From this discussion, it is predicted that a substrate that shows small surface vibration amplitude when in contact with a liquid metal and forms strong bonding as well as small lattice mismatch with liquid layers can trigger highly ordered PNLs

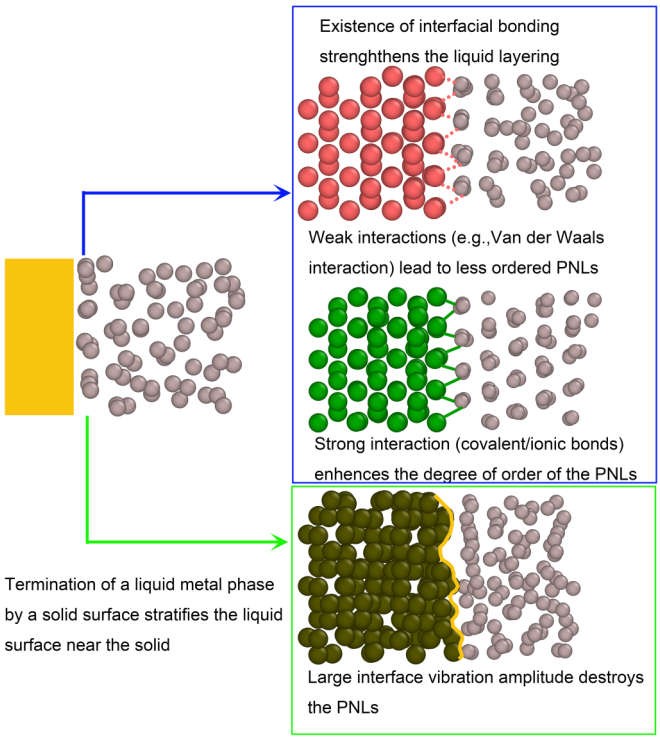

FIG. 18. Schematic diagram showing the role of interfacial bonding and vibration in determining the structural features of a substrate-liquid Al interface.

from the liquid metal. Given that the structural features of the PNLs significantly affect the subsequent heterogeneous nucleation processes, the above three factors, i.e., interfacial bonding strength, interfacial lattice mismatch, and surface dynamical behavior of the substrate, together determine the nature of heterogeneous nucleation of the solid metal phase.

IV. CONCLUSIONS

In this work, AIMD simulations were performed to unveil the influence of interfacial bonding and dynamical behavior on the structural features of the PNLs in the substrate-liquid metal interfaces, which is of critical importance in further understanding heterogeneous nucleation mechanisms. The interfaces of liquid Al and (0001) sapphire surfaces with different surface terminations [(1) nonhydroxylated (0001) sapphire surface including 1Al-terminated, 2Al-terminated, 3O-terminated, and reconstructed sapphire surface; (2) fully hydroxylated (0001) sapphire surface] were studied in detail to probe the PNLs at 950 K and unveil the formation mechanism of the PNLs. Below is the summary of our findings:

The equilibrated interfacial structures at the four nonhydroxylated (0001) sapphire-liquid Al interfaces are the same with the following two typical characteristics: (1) appearance of an Al-rich layer that terminates the sapphire surface; (2) formation of two distinguishable PNLs whose degree of order decay rapidly with increasing distance to the substrate. When the Al-rich layer and the PNL1 are together treated as the surface termination, it is almost identical to the $(\sqrt{31} \times \sqrt{31})R \pm 9^\circ$ reconstructed (0001) sapphire surface,

which supports the previous observation that the presence of liquid Al tends to promote the reconstruction of the (0001) sapphire surface.

The interfacial structure at the fully hydroxylated (0001) sapphire-liquid Al interface is completely different from the interfaces with nonhydroxylated interfaces. The Al-rich layers is replaced by an Al-depletion region, while no distinguishable PNLs are observed.

Interfacial bonding analysis shows that a large proportion of bonds connecting the nonhydroxylated (0001) sapphire substrate and liquid Al are covalent with a strong bonding strength, while the primary interaction at the fully hydroxylated (0001) sapphire-liquid Al interface is the van der Waals force, which is much weaker. The weak bonding strength in the latter case is insufficient to bind the neighboring liquid Al atoms, which is an important reason for the absence of the PNLs at this interface.

Surface dynamical behaviors of the (0001) sapphire substrates in the sapphire-liquid Al interfaces are analyzed. Larger vibration amplitude and higher diffusion ability are found for the atoms at the fully hydroxylated sapphire surface compared to those at the equilibrated nonhydroxylated sapphire surface, which cause a tremendously changing potential energy field in the liquid Al adjacent to the substrate thus impeding the formation of the PNLs.

Formation mechanism of the PNLs at the substrate-liquid metal interface is summarized. In this mechanism, we propose that liquid layering is an intrinsic characteristic of the liquid metal phase when it is brought into contact with a solid substrate, driven by the tendency to increase the coordination number of the liquid atoms in the proximity of the substrate. Meanwhile, the manifestation of the PNLs is determined by a combined influence of the lattice mismatch, bonding strength, and surface dynamical behavior of substrate in the interface: a smaller lattice mismatch, a larger bonding strength between the substrate and the PNLs, and a smaller vibration amplitude and poorer diffusion ability of the substrate surface atoms induce a higher degree of order in the PNLs.

ACKNOWLEDGMENTS

This work was supported by the National Natural Science Foundation of China (Grants No. 51320105003 and No. 51674153). R.L.D. acknowledges support from EPSRC Grant No. EP/N25261/01. S.M. acknowledges the China Scholarship Council for financial support. This research used the ALICE High Performance Computing Facility at the University of Leicester and the supercomputing facilities of National Laboratory for Information Science and Technology at Tsinghua University.

[1] B. Murty, S. Kori, and M. Chakraborty, Int. Mater. Rev. **47**, 3 (2002).
[2] Z. Fan, Y. Wang, Y. Zhang, T. Qin, X. Zhou, G. Thompson, T. Pennycook, and T. Hashimoto, Acta Mater. **84**, 292 (2015).
[3] M. Easton, M. Qian, A. Prasad, and D. StJohn, Curr. Opin. Solid State Mater. Sci. **20**, 13 (2016).
[4] J. Kang, J. Zhu, C. Curtis, D. Blake, G. Glatzmaier, Y.-H. Kim, and S.-H. Wei, Phys. Rev. Lett. **108**, 226105 (2012).
[5] S. H. Oh, Y. Kauffmann, C. Scheu, W. D. Kaplan, and M. Ruhle, Science **310**, 661 (2005).
[6] Q. Zhang, T. Çağın, A. van Duin, W. A. Goddard, III, Y. Qi, and L. G. Hector, Jr., Phys. Rev. B **69**, 045423 (2004).
[7] P. Shen, H. Fujii, T. Matsumoto, and K. Nogi, Acta Mater. **51**, 4897 (2003).
[8] J. Wang, A. Horsfield, U. Schwingenschlögl, and P. D. Lee, Phys. Rev. B **82**, 184203 (2010).
[9] H. Zhang, Y. Han, W. Zhou, Y. Dai, and J. Wang, Appl. Phys. Lett. **106**, 041606 (2015).
[10] J. Sun, D. Wang, Y. Zhang, C. Sheng, M. Dargusch, G. Wang, D. St. John, and Q. Zhai, J. Alloys Compd. **753**, 543 (2018).
[11] A. J. Brown, H. B. Dong, P. B. Howes, and C. L. Nicklin, Scr. Mater. **77**, 60 (2014).
[12] L. Wang, L. Yang, D. Zhang, M. Xia, Y. Wang, and J. G. Li, Metall. Mater. Trans. A **47**, 5012 (2016).
[13] L. Wang, W. Lu, Q. Hu, M. Xia, Y. Wang, and J.-g. Li, Acta Mater. **139**, 75 (2017).
[14] C. Fang and Z. Fan, Comput. Mater. Sci. **171**, 109258 (2020).
[15] Z. Y. Fan, Metall. Mater. Trans. A **44**, 1409 (2013).
[16] F. Mugele and M. Salmeron, Phys. Rev. Lett. **84**, 5796 (2000).
[17] K. Kelton and A. L. Greer, *Nucleation in Condensed Matter: Applications in Materials and Biology* (Elsevier, Amsterdam, 2010), Vol. 15.
[18] W.-S. Xu, Z.-Y. Sun, and L.-J. An, J. Chem. Phys. **132**, 144506 (2010).
[19] K. Sandomirski, E. Allahyarov, H. Löwen, and S. U. Egelhaaf, Soft Matter **7**, 8050 (2011).
[20] S. Dorosz and T. Schilling, J. Chem. Phys. **136**, 044702 (2012).
[21] H. Zhang, S. Peng, X. Long, X. Zhou, J. Liang, C. Wan, J. Zheng, and X. Ju, Phys. Rev. E **89**, 032412 (2014).
[22] H. Zhang, S. Peng, L. Mao, X. Zhou, J. Liang, C. Wan, J. Zheng, and X. Ju, Phys. Rev. E **89**, 062410 (2014).
[23] S. Arai and H. Tanaka, Nat. Phys. **13**, 503 (2017).
[24] C. P. Royall and S. R. Williams, Phys. Rep. **560**, 1 (2015).
[25] A. L. Greer, Nat. Mater. **5**, 13 (2006).
[26] M. Gandman, Y. Kauffmann, C. T. Koch, and W. D. Kaplan, Phys. Rev. Lett. **110**, 086106 (2013).
[27] J. Comtet, A. Niguès, V. Kaiser, B. Coasne, L. Bocquet, and A. Siria, Nat. Mater. **16**, 634 (2017).
[28] H. Men and Z. Fan, Metall. Mater. Trans. A **49**, 2766 (2018).
[29] R. Yan, W. Sun, S. Ma, R. Davidchack, N. Di Pasquale, Q. Zhai, T. Jing, and H. Dong, Comput. Mater. Sci. **155**, 136 (2018).
[30] H. Men and Z. Fan, Comput. Mater. Sci. **85**, 1 (2014).
[31] T. Schülli, R. Daudin, G. Renaud, A. Vaysset, O. Geaymond, and A. Pasturel, Nature (London) **464**, 1174 (2010).
[32] J. P. Palafox-Hernandez and B. B. Laird, J. Chem. Phys. **145**, 211914 (2016).
[33] R. Haghayeghi and M. Qian, Mater. Lett. **196**, 358 (2017).
[34] J. V. Lauritsen, M. C. R. Jensen, K. Venkataramani, B. Hinnemann, S. Helveg, B. S. Clausen, and F. Besenbacher, Phys. Rev. Lett. **103**, 076103 (2009).

[35] S. Ma, A. J. Brown, R. Yan, R. L. Davidchack, P. B. Howes, C. Nicklin, Q. Zhai, T. Jing, and H. Dong, Commun. Chem. **2**, 1 (2019).

[36] S. Ma, R. Yan, T. Jing, and H. Dong, Metals **8**, 521 (2018).

[37] Z. Ma, S. Belyakov, K. Sweatman, T. Nishimura, and C. Gourlay, Nat. Commun. **8**, 1916 (2017).

[38] M. Xu *et al.*, Metall. Mater. Trans. A **49**, 1762 (2018).

[39] C. Fang, H. Men, and Z. Fan, Metall. Mater. Trans. A **49**, 6231 (2018).

[40] J. Du *et al.*, Sci. Rep. **6**, 33931 (2016).

[41] R. Mahjoub, W. Xu, B. Gun, K. Laws, L. Kong, J. Li, and M. Ferry, Comput. Mater. Sci. **108**, 94 (2015).

[42] S. Choudhury, D. Morgan, and B. P. Uberuaga, Sci. Rep. **4**, 6533 (2014).

[43] X. Chen, X.-R. Chen, T.-Z. Hou, B.-Q. Li, X.-B. Cheng, R. Zhang, and Q. Zhang, Sci. Adv. **5**, eaau7728 (2019).

[44] B. L. Bramfitt, Metall. Mater. Trans. B **1**, 1987 (1970).

[45] M.-X. Zhang and P. Kelly, Acta Mater. **53**, 1085 (2005).

[46] M. X. Zhang, P. M. Kelly, M. Qian, and J. A. Taylor, Acta Mater. **53**, 3261 (2005).

[47] H. M. Fu, D. Qiu, M. X. Zhang, H. Wang, P. M. Kelly, and J. A. Taylor, J. Alloys Compd. **456**, 390 (2008).

[48] F. Wang, D. Qiu, Z.-L. Liu, J. A. Taylor, M. A. Easton, and M.-X. Zhang, Acta Mater. **61**, 5636 (2013).

[49] Y. Wang, C. Fang, L. Zhou, T. Hashimoto, X. Zhou, Q. Ramasse, and Z. Fan, Acta Mater. **164**, 428 (2019).

[50] J. Li, L. Wang, X. Zhong, M. Xia, S. J. Haigh, and P. Schumacher, Mater. Charact. **129**, 300 (2017).

[51] H.-T. Li, Y. Wang, and Z. Fan, Acta Mater. **60**, 1528 (2012).

[52] G. V. Kumar, B. Murty, and M. Chakraborty, J. Alloys Compd. **396**, 143 (2005).

[53] Z. Łodziana and J. K. Nørskov, J. Chem. Phys. **115**, 11261 (2001).

[54] D. J. Siegel, L. G. Hector, Jr, and J. B. Adams, Phys. Rev. B **65**, 085415 (2002).

[55] Z. Łodziana, J. K. Nørskov, and P. Stoltze, J. Chem. Phys. **118**, 11179 (2003).

[56] T. Kurita, K. Uchida, and A. Oshiyama, Phys. Rev. B **82**, 155319 (2010).

[57] P. Shen, H. Fujii, T. Matsumoto, and K. Nogi, Scr. Mater. **48**, 779 (2003).

[58] M. Dupraz, R. Poloni, K. Ratter, D. Rodney, M. De Santis, B. Gilles, G. Beutier, and M. Verdier, Phys. Rev. B **94**, 235427 (2016).

[59] H. Reichert, M. Denk, J. Okasinski, V. Honkimaki, and H. Dosch, Phys. Rev. Lett. **98**, 116101 (2007).

[60] I. K. Robinson, Phys. Rev. B **33**, 3830 (1986).

[61] E. Vlieg, J. Appl. Crystallogr. **33**, 401 (2000).

[62] P. J. Eng, T. P. Trainor, G. E. Brown, Jr, G. A. Waychunas, M. Newville, S. R. Sutton, and M. L. Rivers, Science **288**, 1029 (2000).

[63] H. Liang, B. B. Laird, M. Asta, and Y. Yang, Acta Mater. **143**, 329 (2018).

[64] E. A. Jarvis and E. A. Carter, J. Phys. Chem. B **105**, 4045 (2001).

[65] Y. Liu and X.-S. Ning, Comput. Mater. Sci. **85**, 193 (2014).

[66] X.-G. Wang, A. Chaka, and M. Scheffler, Phys. Rev. Lett. **84**, 3650 (2000).

[67] See Supplemental Material at http://link.aps.org/supplemental/10.1103/PhysRevMaterials.4.023401 for model validation, structural evolutions of the nonhydroxylated and hydroxylated sapphire-Al interfaces, and the calculated velocity autocorrelation functions of different interface models.

[68] S. Plimpton, J. Comput. Phys. **117**, 1 (1993).

[69] Y. Mishin, D. Farkas, M. J. Mehl, and D. A. Papaconstantopoulos, Phys. Rev. B **59**, 3393 (1999).

[70] M. Dijkstra, Phys. Rev. Lett. **93**, 108303 (2004).

[71] Y. Duan, J. Li, T. Li, X. Zhang, Z. Wang, and H. Li, Phys. Chem. Chem. Phys. **20**, 9337 (2018).

[72] G. Kresse and J. Hafner, Phys. Rev. B **49**, 14251 (1994).

[73] G. Kresse and J. Furthmuller, Phys. Rev. B **54**, 11169 (1996).

[74] G. Kresse and D. Joubert, Phys. Rev. B **59**, 1758 (1999).

[75] P. E. Blochl, Phys. Rev. B **50**, 17953 (1994).

[76] J. P. Perdew, K. Burke, and M. Ernzerhof, Phys. Rev. Lett. **77**, 3865 (1996).

[77] R. Cavallotti, J. Goniakowski, R. Lazzari, J. Jupille, A. Koltsov, and D. Loison, J. Phys. Chem. C **118**, 13578 (2014).

[78] D. Alfe, Phys. Rev. B **68**, 064423 (2003).

[79] J. Bouchet, F. Bottin, G. Jomard, and G. Zerah, Phys. Rev. B **80**, 094102 (2009).

[80] R. L. Davidchack and B. B. Laird, J. Chem. Phys. **108**, 9452 (1998).

[81] S. T. Lin, M. Blanco, and W. A. Goddard, J. Chem. Phys. **119**, 11792 (2003).

[82] M. P. Desjarlais, Phys. Rev. E **88**, 062145 (2013).

[83] A. D. Becke and K. E. Edgecombe, J. Chem. Phys. **92**, 5397 (1990).

[84] S. A. Chambers, T. Droubay, D. R. Jennison, and T. Mattsson, Science **297**, 827 (2002).

[85] B. G. Walker, N. Marzari, and C. Molteni, J. Chem. Phys. **124**, 174702 (2006).